UNIVERSITY OF SOUTHERN DENMARK

Institute of Biochemistry and Molecular Biology (BMB)

31.08.2015

STED microscopy in human skin

Bachelor project

Author: Irina Iachina
Supervisor: Jonathan R. Brewer
Co-supervisor: Jes Dreier

Abstract

The barrier function of human skin is highly associated to its structure. The structure and the transport pathways of different molecules through the skin are investigated using stimulated emission depletion (STED) microscopy. The STED microscope, a Leica STED SP8, was tested using gold nanoparticles and fluorescent beads. Different pathways and structures of human skin were examined by labeling with the amphiphilic dyes: TopFluor DPPE and ATTO 488 DPPE and with the hydrophilic dyes: Rhodamin B, ATTO 647 N and Abberior Star 440 SX. Investigation and imaging of desmoplakin and keratin 1 were done by immunofluorescence labeling. DMSO as a transport enhancer was tested by measuring the amount of labeling of the skin at different DMSO concentrations. The STED microscope was found to achieve a resolution of 30 nm using fluorescent beads with a diameter of 25 nm. The intercellular lipids in the stratum corneum (SC) labeled with the amphiphilic dyes were resolved down to 100 nm in thickness using STED compared to 200 nm using a confocal microscope, while a resolution of 40 nm was obtained for the immunofluorescence labeled proteins in the skin. Using STED it was possible to resolve the plaques of demoplakin on each side of the intercellular space. The desmoplakin showed pairwise structures with a lower density in the SC compared to stratum spinosum (SS) and stratum basales (SB). The distance between desmoplakin pairs was measured to be 160 ± 30 nm. Keratin 1 was labeled in the corneocytes in the inner part of the SC and the thickness of the corneocytes was measured to be typically 500 nm. DMSO was shown to act as a transport enhancer for TopFluor DPPE at concentrations above 50 % while the opposite was the case for ATTO 488 DPPE. Rhodamin B and ATTO 647 N label both the corneocytes and the intercellular lipids in the SC when these are applied to sliced skin samples, while Rhodamin B only labels the intercellular lipids when applied on intact skin. Both Rhodamin B and Abberior Star 440 SX exhibit a tendency to label keratin in the SG, SS and SB. The results show that Rhodamin B applied to intact skin and Abberior Star 440 SX on sliced samples exhibit tendencies to pass through the skin via the intercellular pathway. The amphiphilic dyes applied on sliced samples exhibit the same tendency, while TopFluor DPPE applied to intact skin does not penetrate the SC. Interestingly Rhodamin B applied to fully hydrated skin sections, was seen to penetrate the intracellular space of the corneocytes suggesting that the hydration of the SC could impair the barrier function and open an intercellular pathway.

Resumé

Menneskehudens barriereegenskab er tæt forbundet med dennes struktur. Dette og transportvejen for forskellige molekyler igennem huden er undersøgt ved hjælp af stimulated emission depletion (STED) mikroskopi fra Leica. STED mikroskopet, et Leica STED SP8 blev undersøgt ved brug af guldnanopartikler samt fluorescerence beads. Forskellige transportveje og strukturen af huden blev undersøgt ved at markere menneskehud med amfifile farvestoffer: TopFluor DPPE og ATTO 488 DPPE og med hydrofile farvestoffer: Rhodamin B, ATTO 647 N og Abberior Star 440 SX. Undersøgelse og afbilding af desmoplakin samt keratin 1 blev udført ved hjælp af immunofluorescencemærkning. DMSO som en transportøger blev undersøgt ved at måle mængden af markering igennem huden ved forskellige DMSO koncentrationer. STED mikroskopet opnåede en opløsning på 30 nm med fluorescerence beads med en diameter på 25 nm. De intercellulære lipidlag i stratum corneum (SC) mærket med de amfifile farvestoffer blev opløst til 100 nm i tykkelse i forhold til 200 nm ved brug af confocal mikroskopi, mens en opløsning på 40 nm blev opnået ved immunofluorescencemærket proteiner i huden. Ved hjælp af STED var det muligt at opløse desmoplakinplader på hver side af det intercellulære område. Desmoplakinen udviste parvise strukturer med en lavere densitet i SC i forhold til stratum spinosum (SS) og stratum basales (SB). Afstanden mellem desmoplakinpar blev målt til at være 160 ± 30 nm. Keratin 1 blev mærket i corneocyterne i den indre del af SC og tykkelsen af corneocyterne blev målt til typisk at være 500 nm. DMSO viste tendens til at virke som en transportøger for TopFluor DPPE ved koncentrationer på over 50 %, mens det modsatte var tilfældet for ATTO 488 DPPE. Rhodamin B and ATTO 647 N labeler både corneocyterne og lipidlagene i SC når disse er påført på skiveskåret hudprøver, mens Rhodamin B kun labeler lipidlagene når denne er påført på intakt hud. Både Rhodamin B og Abberior Star 440 SX udviser tendens til at mærke keratin i SG, SS og SB. Resultaterne viser at Rhodamin B påført på intakt hud og Abberior Star 440 SX på skiveskåret prøver udviser tendens til at passere igennem huden via den intercellulære vej. De amfifile farvestoffer påført på skiveskåret prøver udviser samme tendens, mens TopFluor DPPE påført på intakt hud ikke penetrerer SC. Det er interessant at Rhodamin B påført på fuldt hydreret hud sektioner viste sig at penetrere det intracellulære område af corneocyterne ensbetydende med at hydrering af SC kan forringe barriere egenskaben og åbne en intracellulær vej.

Table of Contents

1. Introduction

The human skin acts as the principal barrier of the body protecting it against physical and chemical harm, includes hindering penetration of molecules. The complex structure of the skin made of lipids and proteins provides the skin with its barrier function. Some skin diseases are thought to be a direct result from either lack of these proteins or alterations of them. For example, it has been observed in mice that if a tight junction protein Claudin 1 is absent death occurs within 1 day due to a lethal water loss. [1] Also diseases like psoriasis and atopic dermatitis are caused by decreased barrier function. [2] This shows that the barrier function of the skin and the structure is highly connected. So in order to understand the former the latter must be investigated. To relieve skin diseases or other illnesses transdermal drug delivery is an important field of research. The transport pathway for certain molecules is therefore of great importance.

Structures in biological samples such as proteins are approximately 5-10 nm is size. So in order to visualize the structure of the skin electron microscopy has been widely used as this can provide a resolution down to 50 pm. [3] The disadvantage of this technique is that experiments must be performed in vacuum making it impossible to visualize biological samples at physiological conditions. This is where super resolution fluorescence microscopy which combines both increased resolution and biological friendly conditions can play an important role. With this technique samples may be investigated at near-physiological conditions. This technique circumvents the classical resolution limit of 200 nm in confocal microscopy and enables a resolution of down to about 10 nm [4] in optimal conditions with for example stimulated emission depletion (STED) microscopy. This type of microscopy is therefore a breakthrough in the fields of bio-imaging. [5]

The structure of the skin is highly connected to the transport pathway of molecules through the skin. Measuring the transdermal diffusion of drugs has mainly been done using either Franz cells [6] or tape stripping [7]. Using Franz cells information regarding the bulk diffusion may be found but the spatial resolution is lost. Tape stripping provides information on the

average penetration of substances at different depths of the skin but this technique is highly invasive and involves destruction of the sample. In this case fluorescence microscopy has an advantage as it enables 3D imaging of the skin without using invasive techniques.

In this project the application of STED microscopy in human skin will be addressed. First the resolution of a STED microscope from a Leica system will be examined using fluorescent beads. The STED microscope will then be used to both examine the structure of the skin and the transport pathway for molecules of different size and affinity. Transport enhancers and their effect on the labeling will also be examined. Skin samples will be labeled with both hydrophilic and lipophilic fluorescent dyes and their location in the skin will give insight into how molecules can penetrate through the skin. It is hypothesized that corneodesmosomes (CD) play an important role in the barrier function and these will therefore be investigated by immunolabeling. The fibrous protein keratin 1 which is an important part of the epidermis will be also be investigated using this technique.

2. Theory

The background regarding both human skin and fluorescence microscopy will be explained in the following.

2.1 Human skin

In order to determine the barrier function of the skin the general structure must be understood.

2.1.1 The structure of human skin

The skin consists of two main layers: the epidermis which is the outermost layer and consists of epithelial cells. This layer varies in thickness from 75 to 150 µm depending on the area of the body. With exception of the epidermis of the palms and foot soles which can be as thick as 0,4 to 0,6 mm. Below the epidermis there is a layer of fiber rich connective tissue which is called the dermis. [8] This project will primarily focus on the barrier function of the skin which is located in the epidermis. The main focus will therefore be on this layer.

Humans shed an amount of skin daily and in order to upkeep the barrier function the epidermis must constantly renew itself. It does so by a process called differentiation. During differentiation the following occurs in random order [9]:

- Synthesis and modification of structural proteins especially a fiber protein called keratin
- New organelles, reorganizing of existing organelles as well as loss of organelles
- Modification of cell size and shape

- Specialization of the cellular metabolism
- Modification of the cell membrane function
- Dehydration

The epidermis itself consists of different layers that are defined by their stage of differentiation. These layers are from the outermost layer (Figure 1): stratum corneum (SC), stratum granulosum (SG), stratum spinosum (SS) and stratum basales (SB). The cells in the epidermis, the epidermal cells are often referred to as keratinocytes due to the fiber protein keratin that is the end product of differentiation. [9, 10]

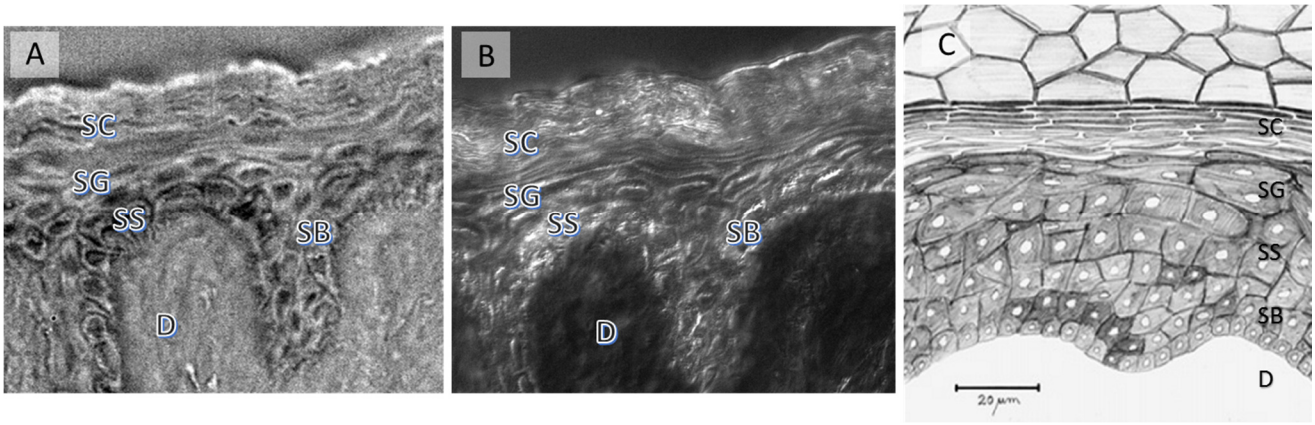

Figure 1: Two images of the same area of the epidermis and a sketch of the epidermis which shows the general structure with stratum corneum (SC) at the top and the subsequent layers below: stratum granulosum (SG), stratum spinosum (SS) and stratum basales (SB). Below SB the dermis (D) is present. The size of A) and B) is 130 times 110 µm A) brightfield image of the epidermis. B) DIC image of the epidermis C) A sketch of the epidermis.

Stratum basales (SB) is the bottom layer of the epidermis. The cells are bound to each other via cross-linked proteins called desmosomes. Desmosomes consist of different proteins some of which are plakoglobin, desmoplakin I and II, desmocollins and desmogleins (Figure 2). [11, 12] The latter two are desmosomal cadherins which are transmembrane proteins that form junctions between neighboring cells. Desmosomes therefore play an important role in connecting neighboring cells as they connect the intermediate filaments of one cell to another. There are subtle structural modifications of the desmosomes as the basal layer differentiates throughout the epidermis. At the bottom of the SB the cell membrane of the cells and their half of the desmosome structures are joined with dermis. This zone of attachment between dermis and epidermis is called the epidermal-dermal junction. Once the cells detach from the dermis they will begin their migration outwards and begin production of keratin 1 and 10. Keratin therefore acts as the intermediate filament in the desmosomes Differentiation of the epidermis is therefore initiated in the SB. The cells in the SB contain stem cells that produce daughter stem cells and transit enhancing cells that are able to undergo many but a finite number of cell divisions. [8]

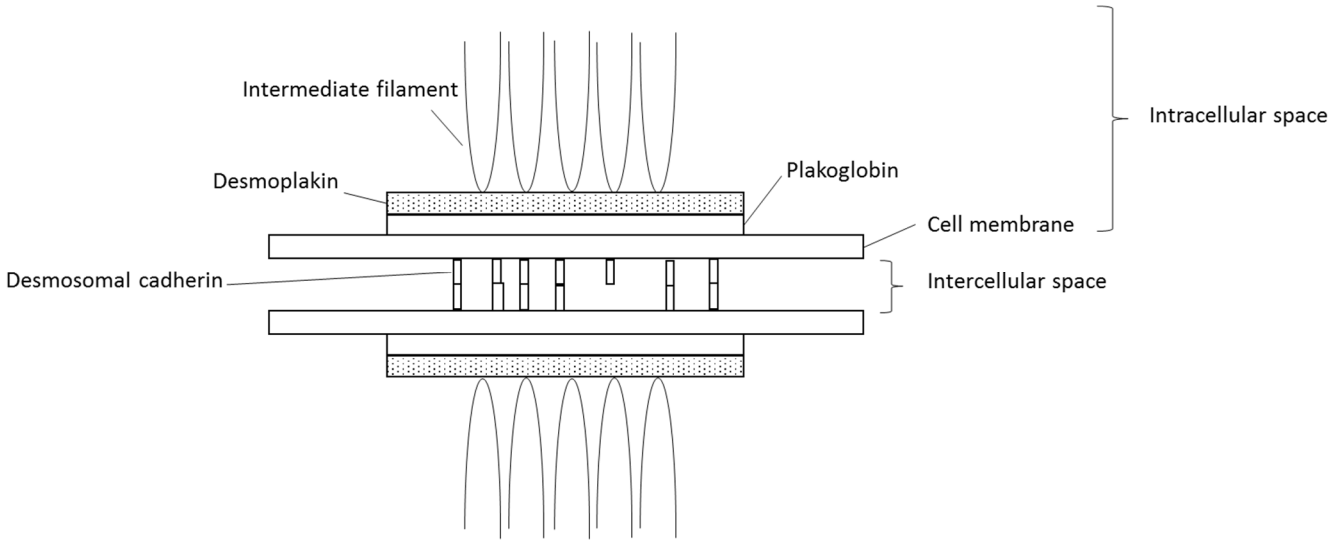

Figure 2: The general structure of the cross-linked protein desmosome that joins two neighboring cells. The two cell membranes are joined in the intercellular space by desmosomal cadherins consisting of desmogleins and desmocollins. In the intracellular space the proteins plakoglobin and desmoplakin are present. Desmoplakin binds to the intermediate filament inside the cell. [11, 12]

Stratum spisosum (SS) consists of migrated dividing cells from the SB. They now take on a polyhedral shape and as the cells migrate outwards they flatten. This layer is several cell layers thick. When the cells are close to the end of differentiation as in at the top of the SS layer a new organelle is formed. [8] These organelles are called lamellar granules (LG) and are about 100 nm times 300 nm in dimensions. It is proposed that they are formed in the Golgi apparatus of the cell and then migrate towards the cells periphery. LG is shown to contain stacks of lipid lamellae consisting of phospholipids, cholesterol and ceramides. [2]

Stratum granulosum (SG) is a layer of flattened cells that are still nucleated. They represent the last layer of living cells before the cornified cells in the stratum corneum. When the granular cells are being transformed into the cells of the SC it is proposed that the LG fuse with the plasma membrane and discharge their lipid lamellae into the intercellular space. [13] Then the short membrane stacks reorganize themselves into lamellar sheets that is the intercellular lipid matrix of the stratum corneum.

Stratum corneum (SC) is the outermost layer of the epidermis and consists of flattened non-nucleated cells. The cells are approximately 40 µm in diameter and 0,5 µm thick. During differentiation all the cellular organelles and cytoplasm are replaced by the fiber protein keratin. These keratin filled cells are called corneocytes. The corneocytes are surrounded by a protein envelope consisting of the cross-linked protein desmosomes, which in the SC have been modified to corneodesmosomes, and furthermore an envelope consisting of covalent bonded lipids. [14] One of the differences between desmosomes and corneodesmosomes is the fact that the intercellular part of desmosomes becomes a homogenous electron dense

desmosomal plate. Due to the binding of desmoplakin in the corneodesmosomes to keratin the corneocytes achieve a highly ordered and dense packing. [8] The corneodesmosomes are therefore highly involved in the intercellular adhesion between adjacent corneocytes and in the cellular organization. The corneodesmosomes become degraded throughout the SC due to soon desquamation which is the detachment of the cells from the epidermis. [15]

As mentioned earlier LG are responsible for creating the intercellular lipid matrix between the corneocytes. By freeze fracture electron microscopy it has been shown that these intercellular areas consist of lipid sheets with several lipid double layers separated by water (Figure 3). The lipid composition in these sheets are: ceramides (40-50% by weight), cholesterol (25%), free fatty acids (10-15%) and other lipids (5%). [2] This particular lipid composition is thought to hold the key to the barrier function of the SC. The free fatty acids and the amide-linked fatty acid chains of the ceramides are saturated and not branched which gives the lipid bilayers a dense packing as well as inducing the lipids into a gel phase. [16] It is thought that cholesterol provides the necessary fluidity to prevent the membrane from becoming too stiff and brittle. [2]

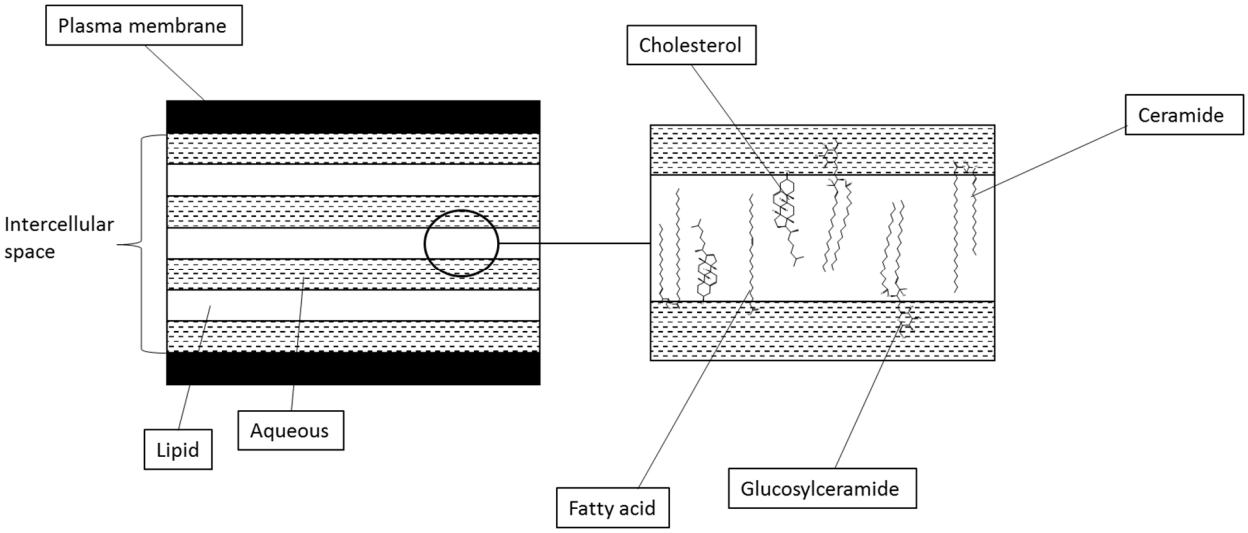

Figure 3: The intercellular space between the corneocytes in the SC. Left: Between two cell membranes several lipid sheets are present that are separated by aqueous regions. Right: a zoom of a lipid sheet showing the presence of a lipid double layer consisting of the following lipids: ceramide, cholesterol, fatty acid and glucosylceramide. [2]

It was earlier thought that the SC was a very porous membrane through which ions and molecules could penetrate and the barrier function of the skin was located in the underlying layers of the epidermis. Later on it was found that these results were misleading due to the treatment applied to the skin prior to experiments for example dehydration, fixation and staining. In 1951 Berenson and Burch showed that the SC was the dominant barrier against water penetration. Blank performed an experiment in 1953 in which he removed layers of the SC until the barrier function of the skin disappeared and several other experiments were

carried out that showed particles remaining in the SC long time after application. All this lead to the new conclusion that the SC indeed possessed the barrier function of the skin. [17]

2.1.2 Transport pathways through the skin

After having a better understanding of the structure of the skin the barrier function is now investigated. The skin's barrier function includes the ability to hinder penetration of molecules of a certain size. It is therefore of interest to determine how molecules with different size and affinity travel through the skin.

Drugs and other substances penetrate the skin by passive diffusion. The skin permeability is described by three parameters: partition coefficient, diffusion coefficient and path length.[18] The partition coefficient for steady flux through the SC also sometimes referred to as the permeability coefficient is described by two physical parameters. One is the thermodynamic parameter describing the molecules affinity for the SC and is typically taken as the partition coefficient between water and octanol. The second and most important parameter of in-tissue mobility is the molecular weight or volume of the molecules, which both can affect if the molecule can penetrate and its penetration rate. [19]

There are three major transport pathways in which particles may diffuse through the skin: 1. Appendage, 2. Intracellular and 3. Intercellular.

Appendage pathways include hair follicles as the most important appendages relative to the surface area of the skin. They can act as transport pathways for percutaneous absorption. But because the skin contains a limited number of hair follicles compared to the surface area of the skin this is not regarded as the dominant path. [20]

The two dominant pathways when looking at transport pathways through the skin are: the intracellular pathway where the particles pass through the corneocytes or the intercellular pathway where the particles travel through the intercellular lipid matrix. It is known that keratin has a high affinity for water and it is proposed that it is the binding of water to keratin that causes the skin to swell during high levels of hydration. [21] Is it therefore expected for hydrophilic molecules to use the intracellular pathway as the corneocytes mainly contain keratin. But as mentioned earlier the intercellular lipid matrix in the SC contains aqueous regions through which hydrophilic molecules also may penetrate the skin. So the pathway for hydrophilic molecules highly depends on the amount of free water in either pathway. Some literature suggests that the swelling of the corneocytes is caused by water binding directly to keratin making the amount of free water within these quite low. [21] It is proposed that free water can only be obtained in very high levels of hydration where it creates pools within the corneocytes destrupting the structure. Due to the low levels of free water in the corneocytes

at a regular level of hydration it is expected for hydrophilic molecules to only use the intercellular pathway but this has not yet been proven. Also when performing experiments with penetration of water through the skin it has been found that the diffusion time is 50 times slower than predicted for the thickness of the SC. This points to the conclusion that water also travels through the intercellular space and not intracellular. [8]

For hydrophobic molecules the predicted pathway is the intercellular as these molecules may use the lipid domains in the lipid matrix of the SC. It is proposed that the lipid regions contain both gel and liquid phases. It is therefore predicted that molecules may use these liquid phases to penetrate the double layers as these are easier to penetrate. [8, 10]

2.1.3 Transport enhancers

In order to enhance penetration of different molecules through the skin transport enhancers can be used. An example of one of these is dimethylsulfoxide (DMSO). DMSO is an aprotic, polar solvent that is miscible with both water and organic materials which makes DMSO able to act as a transport enhancer for many organic and inorganic molecules. [17] Because of the polarity of DMSO it may compete with water for hydrogen bonds with donor molecules for example lipid head groups. During several experiments it has been proven that the increasing transport is dependent on the concentration of DMSO. A significant effect is observed at concentrations above 60 %.

It has been observed in several experiments that water also enhances transport through the skin. The theory is that the water molecules create small hydration shells around the lipid head groups. [22] This causes a less dense lipid packing which makes transport through the lipid sheets easier. The theory behind DMSO's function as a transport enhancer is quite similar. It is proposed that DMSO also creates these hydration shells surrounding the lipid head group but because DMSO molecules do not pack as densely as water molecules the hydration shell is larger. The lipid packing therefore becomes even less dense and the aqueous area between the lipid sheets becomes wider. This will enhance penetration for especially hydrophilic molecules. [17, 22]

A problem with DMSO presents itself during in vitro experiments. After application damage to the skin sample has been observed. [17, 23]

2.2 Light microscopy techniques

Fluorescence microscopy has become an essential tool in many fields of science due to the ability to label specific molecules with fluorescent dyes and then observe a sample under near-physiological conditions.

2.2.1 General principle of fluorescence

When using fluorescence microscopy a sample or a certain part of a sample may be labeled with fluorescent dyes. These consist of fluorescent molecules. A fluorescent molecule must contain a number of highly delocalized electrons, the reason for which will be explained below, meaning the molecules must contain alternating single and double bonds most often in the form of an aromatic system.

In order to explain the reason for the delocalized electrons the states than an electron may occupy must first and foremost be defined. An electron can be in a singlet state where all electrons are spin paired. Alternatively an electron may be in a triplet state where a set of electron spins are unpaired. [24] In order to illustrate these electron states and the transition between these a Jablonski diagram is used which is an energy-level diagram.

In the following the transition from singlet state to singlet state will be described.

When a molecule in the ground state $S_0\ v'' = 0$ (Figure 4A) absorbs a photon, the energy of the photon will excite the molecule typically into a higher vibrational level of a higher electron energy level, for example $S_1\ v'' > 0$. First the molecule loses some of the excess energy by vibrational relaxation to the lowest vibrational state of the excited state $S_1\ v'' = 0$. This process occurs within femto- to picoseconds. Afterwards there are different pathways from which the molecule can release the remaining excess energy. [25]

One of these pathways is that the molecule relaxes from the lowest energy vibrational state of the excited state S_1, usually to a vibrational energy level $v'' > 0$ in the S_0 state. This relaxation can happen with the release of energy in the form of a photon and is called fluorescence. The molecule then loses the rest of the excess energy by vibrational relaxation to ground state in $S_0\ v'' = 0$. The energy of the absorbed photon is therefore most often higher than the fluorescent photon. [25] The shift in energy between the absorbed and emitted light is called the Stokes shift and is important for separating the excitation light from the emitted light in fluorescence microscopy. [25]

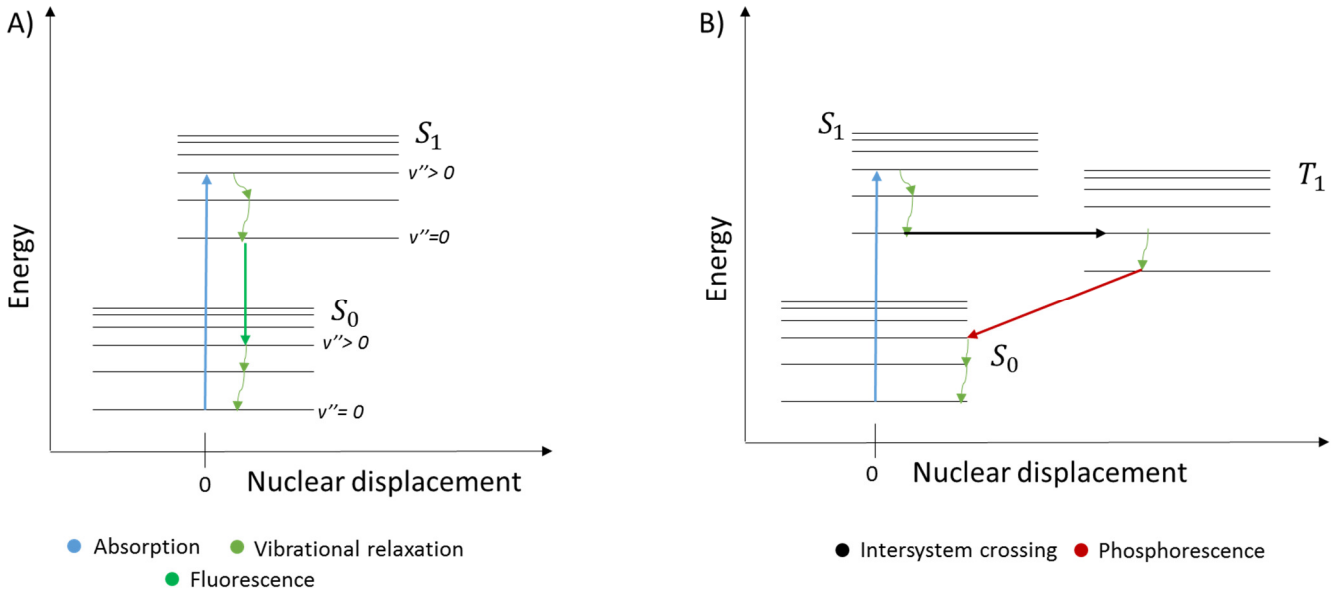

Figure 4: Jablonski diagram representing different processes a molecule may undergo after excitation. A) Jablonski diagram showing the process fluorescence. The molecule is excited from $S_0\ v'' = 0$ by a photon (blue) to $S_1\ v'' > 0$. The molecule then loses some of the excess energy by vibrational relaxation (light green). When the molecule is in $S_1\ v'' = 0$ the molecule will lose most of the excess energy by relaxation to $S_0\ v'' > 0$ and emitting a photon (green). B) Jablonski diagram showing the process phosphorescence. The molecule is excited from $S_0\ v'' = 0$ by a photon (blue) to $S_1\ v'' > 0$. The molecule then loses some of the excess energy by vibrational relaxation (light green). When the molecule is in $S_1\ v'' = 0$ the electron's spin is flipped and it makes a transition into a triplet state T_1 by a process called intersystem crossing (black). After milliseconds the molecule relaxes back into the singlet state $S_0\ v'' > 0$ by emitting a visible photon by a process called phosphorescence (dark red).

The transition from singlet state to triplet state will now explained. Another option is when a molecule has been excited to $S_1\ v'' = 0$ the electron's spin flips which leads to a transition to a triplet state, a so called intersystem crossing (Figure 4B). If a molecule ends up in a triplet state it will stay in this condition for a longer period of time as the transition from triplet to single state is less probable. When the molecule is in the triplet state it may lose the excess energy as heat by relaxation to the ground state or it may emit a visible photon. The latter process occurs slowly (in milliseconds, compared with fluorescence that occurs within nanoseconds) and is called phosphorescence. The transition from a singlet state into a triplet state is more favorable if there is a large overlap between the wave functions of the vibrational levels in the excited singlet state, S_1 with the wave functions of the vibrational levels in the triplet state, T_1. [24, 25]

2.2.2 Resolution and diffraction limits

In fluorescence microscopy several lenses are used due to their ability to focus parallel beams onto a single spot and magnify an object. So the property of lenses when regarding light emitting objects must be understood.

When looking at a light emitting object through a lens a single point will not be observed. Due to the wave properties of light diffraction will occur when the light is scattered on the edges of the lens. This will cause a so called Airy Disk to be seen which has the highest light intensity in the middle and then alternating zero and non-zero decreasing intensities outwards. The area between the center of the disk and the first zero intensity ring corresponds to the distance from the optical axis where rays from one side of the lens are out of phase with rays from the other side of the lens. It therefore evident that the size of the disk depends on the size of the lens or more precisely how much of the total light the lens can collect.

The radius of the Airy Disk is given by the following equation [24]:

$$r = \frac{0.61\,\lambda}{\sin\theta} \qquad (2.1)$$

Where θ is the half acceptance angle of the lens (Figure 5). If the object in question is smaller than the Airy Disk it becomes problematic because then all information regarding the object's size and shape disappears.

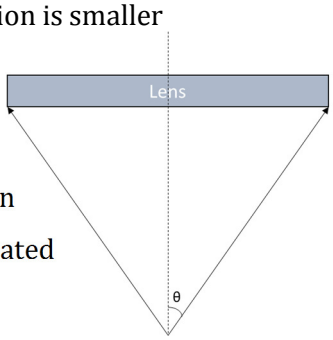

Figure 5: The half-acceptance angle of the lens θ which is the half angle between the optical axis and the edge of the lens.

A 3D representation of a light emitting spot is called the point spread function (PSF). The horizontal view of the PSF will appear as the Airy Disk and as an elongated ellipse in the vertical view [24].

When using a light microscope one most often looks at more than one illuminating point. The resolution of a microscope is defined by the ability to distinguish between two points. Rayleigh claimed that it is possible to distinguish between two Airy Disks if the center of one hits the first minimum of the second.

Or if two points are separated by a distance *d*, then we may able to distinguish between the two if *d* is larger than or equal to the radius of the Airy Disk. Equation (2.1) may therefore be used to predict the resolution of a microscope by regarding *d* as the minimum resolved distance.

Rayleigh's approach is useful when looking at fluorescent molecules that may be regarded as individual points. But if an area that has been stained with fluorescent molecules are illuminated by the same source the points can no longer be viewed as being independent. [24]

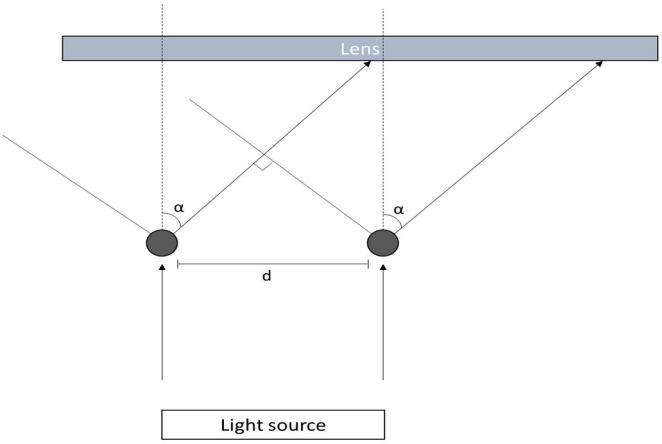

Figure 6: Two points separated by a distance *d* are illuminated with parallel rays from the same light source. The light diffracts in all directions from each point. Only the light diffracted in a certain direction at an angle α is shown.

As mentioned earlier light that hits a small object or the edge of a larger object will be diffracted ergo spread in all directions. Now imagine a finite number of points separated by the same distance d illuminated by parallel light rays (Figure 6). Every point will spread light in every direction. If looking at a particular direction at an angle α the light rays will all be displaced by a distance r. If $r = \frac{\lambda}{2}$ destructive interference will occur when the light rays of this particular angle meet and this area will appear dark upon looking at the back focal plane of the lens. On the other hand if $r = \lambda$ or any integer $n\lambda$ constructive interference will occur and there will be light in this area. So on the back focal plane of the lens one sees alternating light and dark areas which is called a diffraction pattern. Based on this it may be predicted that the path difference λ equivalent to the smallest diffractions angle that will result in constructive interference is [24]:

$$\lambda = d \sin \alpha \tag{2.2}$$

Objects may be thought of as a collection of several points. Ernst Abbé stated that an un-diffracted ray does not provide any information about the sample as this ray has passed in between the points. [24] So in order to gather information about the sample the diffracted rays must be able to enter the lens. If $\sin \alpha$ is small enough for the ray to enter the lens then two points can be separated. If not the two points are indistinguishable. From this it is apparent that the half acceptance angle of the lens, θ is of importance (Figure 5). If $\alpha > \theta$ the diffracted light will not be able to enter the lens and if $\alpha = \theta$ it will. A limiting value of d (the minimum resolved distance) when $\alpha = \theta$ is achieved [24]:

$$d = \frac{\lambda}{\sin \theta} \tag{2.3}$$

If the sample is illuminated with a converging light beam with a half angle that is equal to or larger than θ instead of parallel light beams the situation changes (Figure 7). Now it is possible for diffracted light where $\alpha = 2\theta$ to enter the objective lens.

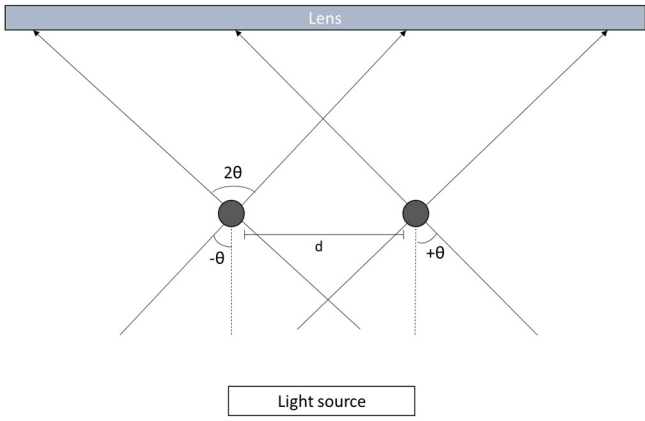

Figure 7: Two points separated by a distance *d* are illuminated with converging rays from the same light source. The diffracted light with an angle up to 2θ can enter the lens.

This results in an equation for the minimum resolved distance which is also called Abbe's formula for the resolution of a microscope lens [24]:

$$d = \frac{\lambda}{2 \sin \theta} \tag{2.4}$$

Where d is the minimal resolved distance also called the diffraction limit and λ is the wavelength of the incident light. From (2.4) it is evident that a lower wavelength will result in a larger microscope resolution.

The wavelength of the light is dependent on the frequency of the light and the velocity by this equation $v = f\lambda$. Light has a lower velocity in a denser material than in vacuum and air and is it therefore important to determine how much slower this is. For doing so the refractive index, n is introduced which is the ratio of the speed of light in the chosen medium to its velocity in vacuum or air. Usually the sample in question is placed inside a medium for example glass (n=1,5) in which the velocity of light is lower and the wavelength is therefore shorter. To improve the resolution the high refractive index must go all the way to the lens for which an immersion fluid is used for example oil (n=1,515). With this in mind (2.4) becomes [24]:

$$d = \frac{\lambda}{2n \sin \theta} \tag{2.5}$$

Where $n \sin \theta$ is the numerical aperture of the lens, NA. In light microscopy the wavelength of the excitation laser is in the visible region which is in the range of 400-700 nm and the numerical aperture for an oil objective is $NA_{oil} = 1{,}44$ which gives a maximum resolution of approximately 200 nm in the xy-direction. In the z-direction the resolution is given by the following equation [26, 27]:

$$d_z = \frac{2\lambda}{n \sin^2 \theta} \tag{2.6}$$

Given the same conditions as in the xy-direction and looking at a sample with few clearly defined particles the resolution in the z-direction becomes approximately 500 nm. There is no optical sectioning in a sea of dye.

2.2.3 Fluorescence microscopy:

The setup of a general fluorescence microscope is going to be explained in the following (Figure 8 – without the pin-hole aperture). First the excitation laser is expanded by a set of lenses. The lenses are chosen so the diameter of the expanded light corresponds with the back aperture of the microscope objective as the best resolution is achieved when the entire back aperture is illuminated. The light is then reflected by a dichroic mirror that has the ability to reflect or transmit light with distinct wavelengths. In this case the dichroic is chosen to reflect the excitation light and transmit the emitted fluorescence. The sample is illuminated and the fluorescence light is passed back in the same direction as the excitation beam. As mentioned earlier the fluorescence wavelength is larger than the excitation wavelength, and the fluorescence light can therefore be separated from the excitation light by the dichroic mirror. The fluorescence light may then be focused by another set lenses in order to collect the light with a detector. [25] The detector could be a CCD camera or in the case of a laser scanning microscope a point detector such as a PMT.

2.2.4 Confocal microscopy:

When using conventional fluorescence microscopy the detector will receive light from points in the sample that are not in focus. In order to separate the out-of-focus light from the in-focus light a pin-hole aperture is placed in front of the detector (Figure 8). This enables only collecting light from the focal excitation region as only this can pass through the pinhole. Light from other excitation regions will be either fully or half suppressed by the pin hole. The laser acts as another pin hole on the sample. [24]

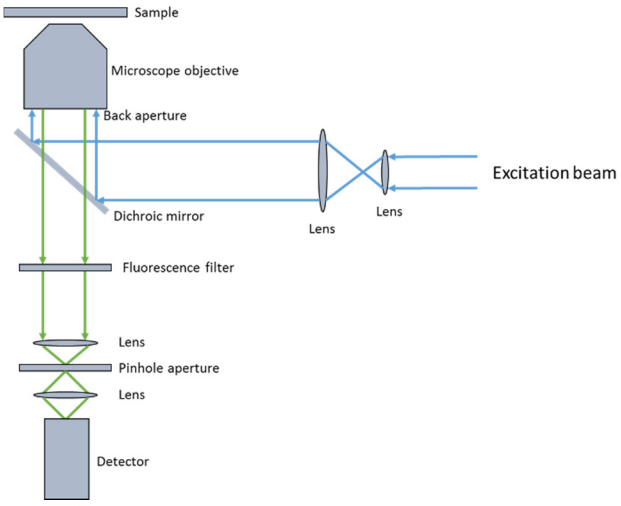

Figure 8: General set-up of a confocal microscope. The excitation laser (blue) is first expanded by a set of lenses so the width of the light matches the back aperture of the microscope objective. The light is reflected from a dichroic mirror and enters the microscope objective. The fluorescent light (green) then passes through the dichroic mirror and a fluorescence filter that filters out any excitation light. The fluorescence light is then focused into a pin-hole aperture by a lens into to filter out any out-of-focus light. The light is then focused into a detector by another lens.

In order to capture an image of the entire sample it is necessary to scan the entire sample. If scanning mirrors are placed only in the pathway of the excitation laser the fluorescent light will

not be able to pass through the pin hole. The microscope set-up is therefore chosen so that the excitation laser and the fluorescence use the same pathway and therefore pass the scanning mirrors while these are in the same position. This enables scanning of the entire sample while maintaining the pin-hole concept. When the light going to and from the sample use the same pathway it is called d-scan. This approach is based on assuming that the light will behave perfectly for example not scattering inside the sample.

The pin hole provides a resolution volume of 200-300 nm in the xy-direction and approximately 500 nm in the z-direction. The pin-hole determines the resolution in the z-direction as it is the amount of suppressed out-of-focus light that determines the resolution. The amount of suppressed light depends on the area of the point that is out of focus projected onto the pin-hole. The area of the point is determined by the numerical aperture of the objective. The diameter of the point is therefore determined directly by the numerical aperture and the area of points is determined by $(NA)^2$. It is therefore necessary to use objective lenses with a high numerical aperture rather than a high magnification in order to achieve good quality 3D images. [24]

As mentioned above the resolution limit of a conventional and confocal fluorescence microscope is around 200 nm in the xy-direction limiting the exploration of smaller objects. To solve this problem so called nanoscopes are introduced. The principle behind these kinds of microscopes to control the excitation so that only a sub diffraction limited spot is excited. Thus the location of the sub diffraction limited objects can be distinguished and then combined to create a full super resolution image.

In 2014 Thomas Ebbesen, Sir John Pendry and Stephan Hell received the Nobel Prize in chemistry for the development of a super resolution fluorescence microscope: “stimulated emission depletion (STED) microscope” [5]. The technique behind the microscope enables us to control when the different points within a sample emit or do not emit light. This has revolutionized the world of microscopy by being able to achieve a resolution down to 10 nm [4].

2.3 STED microscopy

As mentioned earlier when a molecule is excited to an excited state there are different pathways for the molecule to lose its excess energy. When the molecule has relaxed to $S_1\ v'' = 0$ the molecule may be forced to $S_0\ v'' > 0$ (Figure 9) by a process called stimulated emission. This is done by illuminating the excited molecule with a photon, STED photon with an energy corresponding exactly to the energy difference between $S_1\ v'' = 0$ and $S_0\ v'' > 0$. This will

force the molecule into the ground state $S_0\ v'' > 0$ and it will emit a photon with the exact properties of the STED photon. Thus the STED photons are said to de-excite the molecules. The molecules in the $S_0\ v'' > 0$ state then quickly relax to the $S_0\ v'' = 0$ state. [25]

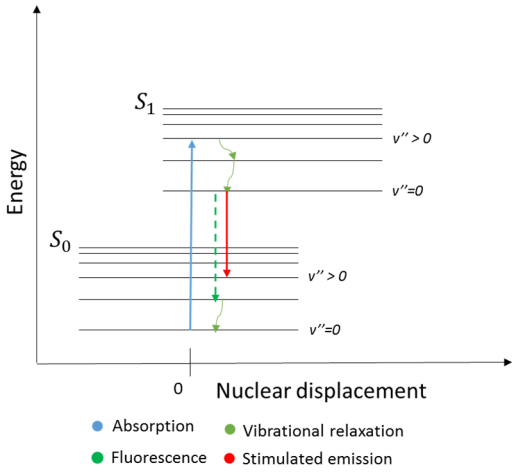

Figure 9: Jablonski diagram showing stimulated emission. The molecule is excited from $S_0\ v'' = 0$ by a photon (blue) to $S_1\ v'' > 0$. The molecule then loses some of the excess energy by vibrational relaxation (light green). When the molecule is in $S_1\ v'' = 0$ a STED photon is emitted onto the sample which has the exact same energy as the energy difference between $S_1\ v'' = 0$ and $S_0\ v'' > 0$. This will force the molecule in to the latter energy state and emit a photon with the same properties as the STED photon (red). Fluorescence is also depicted (green, dashed).

2.3.1 Characterization of STED set-up and resolution

The STED microscope is built from the same principal as a confocal microscope. The difference is the addition of a STED laser that also illuminates the back aperture of the objective (Figure 10).

The STED laser passes through a dichroic mirror that only reflects the light from the STED laser. An optical component called a phase plate is placed in front of the optical route of the STED laser. The phase plate works by creating an interference pattern which form the STED laser into a torus shaped beam (Figure 11A). The result is that the STED laser depletes the fluorescence excitation except in the central dark spot of the STED beam. The PSF of the fluorescence light and that of the STED laser are combined by saturated depletion (Figure 11C). The amount of light from the fluorescence that can be seen in the zero point of the STED pattern is then the effective PSF. Effectively this means that the light emitted within the donut, but not the center, is turned off while the light in the zero point is not.

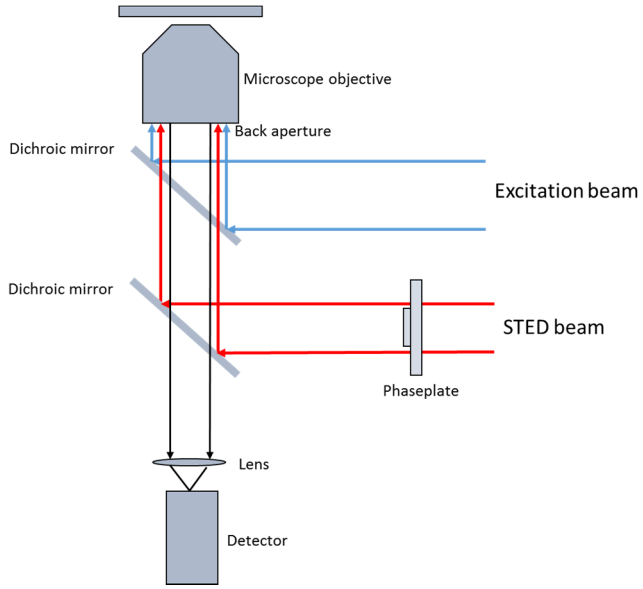

Figure 10: The general set-up of a STED microscope. The set-up is the same as in Figure 8 with the addition of a STED laser (red) and a phase plate. The phase plate interferes with the waves of the STED laser and creates destructive interference at the center of the PSF. The STED beam is reflected by one dichroic mirror and transmitted through another in order to enter the objective lens. Fluorescence (black) then travels through both dichroic mirrors and into a detector.

As it is necessary to first excite the molecule and then de-excite them before they release their energy by fluorescence time

dependent pulses must be applied. If a detector is set to catch the light directly after excitation the detector will only detect the fluorescence. If instead the detector is set to catch light after the STED laser has been activated the detector will only detect light from the central spot created by the phase plate. [25]

The resulting PSF is smaller but it is not the main reason for the increased resolution. What gives STED the increased resolution is the saturation factor. Meaning that if the intensity of the STED laser is increased in the same area the depleted area will become saturated meaning there are no more molecules to de-excite. The increased amount of photons will now also be able to de-excite molecules further towards the central spot of the PSF. This will cause the boundaries of the depletion zone to move further into the center. Theoretically the result is an almost infinite high resolution but the diameter of the resulting spot depends on the photo physical properties of the fluorescent dyes as well as the intensity of the STED laser [24].

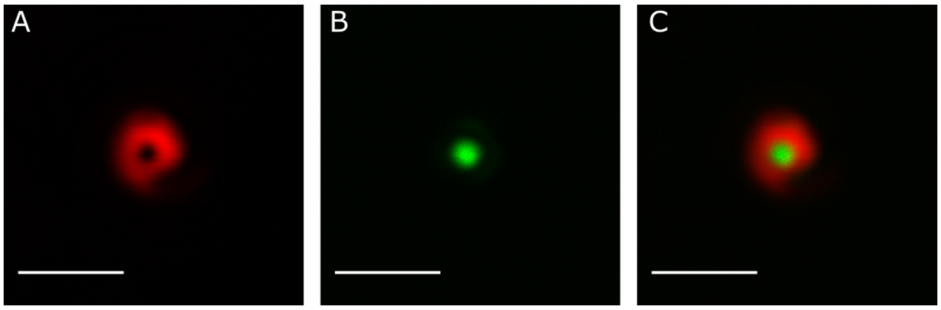

Figure 11: Examples of PSFs of the excitation laser and the STED laser.
A) The PSF of the STED laser B) The PSF of the excitation laser C) The two PSFs combined. Scalebar is 1 µm.

The diffraction limit described by Abbé (2.5) is still valid, but can now be modified to accompany the new variables in the system [28]:

$$d = \frac{\lambda}{2n \sin\theta \sqrt{1 + I_{sted}/I_s}} \tag{2.7}$$

I_{STED} is the incident power of the STED laser and I_s is the saturation intensity at which exp(-1) (about 37%) of the molecules are not depleted. And $\frac{I_{sted}}{I_s}$ is defined as the saturation level. From (2.7) it is clear that with an increasing power of the STED laser the diffraction limit can be almost infinitely lowered. [28, 29]

3. STED microscopy in human skin

3.1 Materials and methods

The general theory regarding skin structure and fluorescence microscopy is now combined and tested by performing several experiments to examine the response of the Leica STED microscope, the structure of the epidermis and the transport pathway through the skin.

3.1.1 Materials

The fluorescent dyes used in all the following experiments were: 1-palmitoyl-2-(dipyrromethene boron difluoride)undecanoyl-*sn*-glycero-3-phosphoethanolamine, TopFluor DPPE (Avanti Polar Lipids, USA), ATTO 488 DPPE (ATTO TEC, Germany), ATTO 647N (ATTO TEC, Germany), Rhodamin B (Sigma-Aldrich, Denmark), Abberior Star 440 SX (Abberior, Germany). The antibodies used for immunolabeling were: primary antibodies: Anti-Desmoplakin I+II antibody mouse, AB16434 (Abcam, USA), Anti-Cytokeratin 1 antibody rabbit, AB24643 (Abcam, USA). Secondary antibodies: Abberior Star 440 SX Goat anti-mouse IgG (Abberior, Germany), Abberior Star 488 Goat anti-rabbit IgG (Abberior, Germany). Fluorescent beads used in preliminary experiments: 20 nm yellow-green (Life Technologies – Invitrogen, Denmark), 25 and 47 nm (Thermoscientific – particle technology, Denmark). Tissue Tek used in order to cryofreeze skin samples (Sakura Finetek, Denmark). PBS buffer (in pill form) and all other chemicals used were from Sigma-Aldrich (Denmark). And finally the embedding medium used in all experiments: ProLong Gold antifade reagent (Life Technologies, Denmark)

3.1.2 Skin

In the following experiments human skin samples were used that were obtained from operations on breast reduction and abdominoplasty. Non colored (without curcumin) ethanol iodide was used for disinfection during the surgery. The samples were used 24–48 hours after surgery. The experiments performed in this work, involving the use of human samples, were approved by the Regional Research Ethics Committee of Southern Denmark, and were adherent to the Declaration of Helsinki Principles (2008). Patient consent for experiments was not required, because Danish regulations consider human tissue left over from surgery as discarded material.

Samples were trimmed into 0.5–1 mm-thick 1 cm^2 sections, washed in tap water, patted dry on the surface, and placed with the SC side up on a PBS-wetted filter paper. The skin samples were then cryofrozen using the protocol described in Appendix 1, Protocol 1.

3.1.3 Samples for characterization of the STED set-up and its resolution

In order to examine the shape and overlap of the point spread function of the STED laser and excitation laser of the Leica system, samples of gold nanoparticles were prepared. The protocol for preparation of these can be seen in Appendix 1, Protocol 2. Beforehand coverslips were cleaned in basic piranha (Appendix 1, Protocol 3). All coverslips used in all the experiments were type #1,5 corresponding to a thickness of 0,17mm . In order to examine the resolution of the Leica STED system samples of fluorescent beads were prepared. The beads were prepared using the protocol seen in Appendix 1, Protocol 4 and the bead solutions were applied to coverslips that were washed in ethanol and dried under N_2. Three different bead sizes were used: 20, 25 and 47 nm. All of these were prepared in concentrations 1:5.000 and 1:50.000, the 20 and 25 nm beads were also made in the concentration 1:1.000.000 and last the 47 nm beads were also made in a concentration of 1:100.000.

3.1.4 Affinity labeling of human skin

In order to optimally image the structure of the epidermis several preliminary experiments were performed to determine the ideal sample thickness and labeling protocol, including determining the optimal DMSO concentration needed in order to achieve the highest amount of labeling. The fluorescent dye concentration was 8 µM in all the following experiments. The first fluorescent dye to be tested was TopFluor DPPE. Solutions containing 10 mL each were made by adding the appropriate amount of 10mM PBS buffer and DMSO to achieve the desired DMSO concentration. The dye was then dissolved in the following DMSO concentrations: 0, 5, 10, 20, 30, 50 and 100 %. Skin samples were cut in 30 µm sections using a cryotome from Thermo Scientific, collected on Super Frost Plus microscope slides and then labeled using the following protocol:

Protocol (1) for labeling human skin:

Buffer used: 10 mM PBS buffer in milliQ water.

1) After sectioning the sample is fixed for 10 min in -20˚CMeOH
2) Rinsed twice with 1 mL of buffer
3) A hydrophobic magic marker is then used to draw a circle around the sample.
4) 100 µL of dye solution is added and the sample is left overnight.
5) The dye is removed and the sample is rinsed at least 3 times in buffer.
6) 150 µL buffer is added for 15-30 min
7) The water is removed(repeat step 4-7 if a second dye is to be applied)
8) Add embedding medium (Prolong Gold) and cover glass

After circa 24 hours the samples could now be imaged using the Leica system. The experiment was repeated with DMSO concentrations of: 60, 70 and 85 % and skin samples cut into 20 µm sections as well as with DMSO concentrations of 5, 30 and 100 % and section thicknesses of 10 and 30 µm.

Similar experiments were performed with the fluorescent dye ATTO 488 DPPE. Here the used DMSO concentrations were: 0, 5, 30 and 100% and the skin samples were cut in 20 µm slices.

Several samples using both ATTO 488 DPPE and TopFluor DPPE were then prepared to investigate the structure of the epidermis. The latter was dissolved in 100 % DMSO and ATTO 488 DPPE was dissolved in 100 % PBS buffer. Skin samples were cut in 20 µm slices and the labeling was done following protocol (1). Both confocal and STED images were taken in order to compare the thickness of the lipid sheets in the SC.

A similar labeling optimization was carried out with the following hydrophilic dyes: Rhodamin B, ATTO 647 N and Abberior Star 440 SX. With all the dyes two different samples were made, one where step 6) in protocol (1) was performed and one where it was not.

3.1.6 Duel labeled samples with hydrophilic and hydrophobic dyes

In order to examine the transport pathway through the skin it is interesting to label a sample with both hydrophobic and hydrophilic dyes. As the hydrophobic dye TopFluor DPPE is applied dissolved in 100 % DMSO the effect of DMSO on the hydrophilic dye Rhodamin B was examined. Skin samples were sliced in 20 µm slices and prepared using protocol (1). The first sample was prepared by first applying DMSO as the primary dye and then Rhodamin B. The second sample was prepared by applying DMSO, after application of Rhodamin B.

Samples were also prepared using protocol (1) were the primary dye application was the hydrophobic dye TopFluor DPPE dissolved in 100 % DMSO while the second dye application was Rhodamin B and ATTO 488 DPPE dissolved in 100 % PBS buffer. Another set of samples were prepared with the dye application in the reverse order.

The same procedure was then followed using the hydrophilic dye Abberior Star 440 SX and ATTO 488 DPPE in 100 % PBS buffer as the primary dye solutions and TopFluor DPPE in 100 % DMSO as the second.

3.1.7 Samples labeled before sectioning

Samples were also made where the fluorescent dye was applied before slicing meaning before the skin sample was cryofrozen. The fluorescent dyes Rhodamin B and TopFluor DPPE were both dissolved in 100 % DMSO in order to achieve a dye concentration of 0,1 M. Then 40 µL dye solution was placed on a 1x1 cm skin sample overnight at 5°C with an un-rinsed coverslip

on top. The excess dye was then removed and the sample was rinsed with 2x1 mL of PBS buffer. The skin samples were then cryofrozen (Appendix 1, Protocol 1). The samples were cut into 20 µm sections and then mounted directly onto the coverslips cleaned in basic piranha (Appendix 1, Protocol 3) and prepared for skin mounting (Appendix 1, Protocol 5) and then mounted using Prolong Gold as embedding medium.

An intact sample labeled with Rhodamin B was also sliced in 20 µm slices and prepared using protocol (1) but solutions of TopFluor DPPE dissolved in 100 % DMSO and ATTO 488 DPPE dissolved in 100 % PBS buffer were also applied to the sample.

3.1.5 Antibody labeling

In order to examine specific proteins in the epidermis the skin samples were labeled by immunofluorescence labeling. This procedure in short involves tagging specific antigens within the sample with a specific antibody (immunoglobulin). This is the primary antibody. Then a secondary antibody is selected that then tags the primary antibody and is also labeled with a fluorescent tag making the antigen visible via fluorescence microscopy (Figure 12). [24, 30] The protocol for immunolabeling can be seen below (Protocol (2)). In order to image the desmosomes the protein desmoplakin was stained. The primary antibody used was anti-Desmoplakin I+II antibody mouse, AB16434. The secondary antibody was goat anti-mouse IgG anti mouse and labeled with the fluorescent tag Abberior Star 440SX.

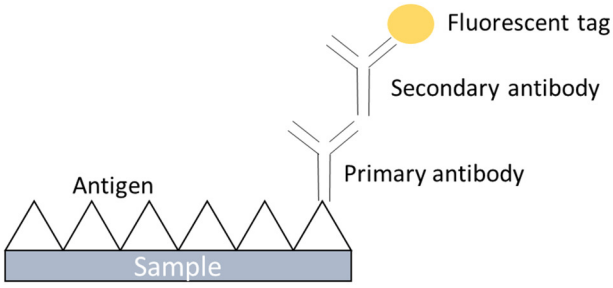

Figure 12: The principal behind immunolabeling which enables labeling of distinct proteins within a sample. Antigens within the sample are tagged by a primary antibody which is then tagged by a secondary antibody. The latter is labeled with a fluorescent molecule.

All samples prepared for STED microscopy were prepared directly on coverslips and not on microscope slides. The cover slips were therefore cleaned in basic piranha (Appendix 1, Protocol 3) and prepared for mounting of the skin sample as described in (Appendix 1, Protocol 5).

Protocol (2) for immunolabeling of human skin:

PBS/BSA/SA solution used: 10 mM PBS buffer in MilliQ water, 10 mg/mL BSA, 0,5 mg/mL sodium azide.

1) Skin was cut into 20 µm sections using a cryotome from Thermo
2) After slicing samples were immersed for 10 min at -20ºC in MeOH
3) Then rinsed with 1 mL of running buffer

4) A hydrophobic magic marker is then used to draw a circle around the sample.
5) Then wash with approx. 100-200 µL PBS/BSA/SA for 2x5 min.
6) Block with PBS/BSA/SA for 1 hour
7) Add diluted 1:200 primary antibody (incubate overnight at 4°C)
8) Wash with PBS/BSA/SA for 3x5 min.
9) Add diluted 1:200 secondary antibody (incubate 90 min. at 37°C or overnight at 4°C)
10) Wash with PBS/BSA/SA for 3x5 min.
11) Add immersion media (Prolong Gold) and mount.

The sample was then ready to be examined using the Leica system. Samples with labeled keratin 1 were prepared in the same manner. Here the primary antibody was anti-Cytokeratin 1 antibody rabbit, AB24643. The secondary antibody was goat anti-rabbit IgG labeled with the fluorescent tag Abberior Star 488.

3.1.8 Confocal and STED microscopy

The microscope used for confocal and STED imaging was a Leica SP8 (Manheim, Germany). The excitation laser used was a pulsed white light. The STED laser was a CW laser at 592 nm. The system was equipped with a hybrid detector and used gated detection. Images were collected using both the galvo scanners and the resonant scanners. A 100X oil objective (NA=1,40) lens was used in all the measurements. Typically a stack of 6-10 images were recorded with a pixel size of between 15-30nm and a z step of 150nm. STED laser power was typically 20-50%.

3.1.9 Deconvolution

Deconvolution of acquired images and stacks was done using Huygens professional (Scientific Volume Imaging, Holland). In short deconvolving is the opposite of convolving which happens when an image of a sample is recorded. Fluorescent spots within the sample are convolved into PSFs and the resulting image will show the spots as PSFs. Deconvolve is therefore the opposite process were a real-life image of a sample is created from the captured image (Figure 13). [24] Further explanation is beyond the scope of this assignment.

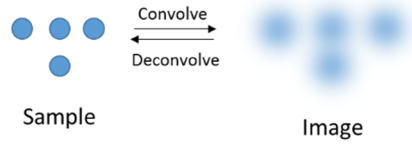

Figure 13: Light emitting points are convolved into PSFs in the resulting image. The reverse process is where the image is deconvolved into a real-life image of the sample.

3.2 Results and discussion

The results from the experiments described above will now be described and discussed.

3.2.1 Characterization of STED set-up and resolution

In order to examine the microscope set-up and the PSF's of the lasers use gold nanoparticles can be used as these have the property to reflect light. So in this experiment the reflection of

the excitation laser and the STED laser of the Leica system were examined. Images were captured in both the xy- and xz-direction using the Leica system. Subsequent all the images were edited with Fiji ImageJ. When looking at the reflection of the excitation laser in the xy-direction (Figure 14B) the PSF does not appear as an Airy Disk. The PSF appears mainly as a single bright spot due to the fact that the secondary maximum after the first minimum of the Airy Disk is only 1,7% of the light [24]. The diameter of the PSF was measured and found to be at around 200 nm which confirms the calculation of the resolution from equation (2.5). Then the PSF of the STED laser is examined (Figure 14A). As expected this has the characteristic donut shape in the xy-direction with an intensity of approximately zero in the center. However a lower intensity in the lower right side of the donut was observed in all the experiments. This can also be seen in Figure 15 where a graph of the normalized intensity profiles can be seen. The intensity profile of the STED laser (red) shows that the intensity at the center of the donut is not zero, which it ideally should be. In fact the ratio between the intensity at the center of the donut and the lowest side lobe is about 0,16. This will of course induce some unwanted stimulated emission from the center of the donut resulting in a reduced intensity from the sample. The cause of this and the non-symmetric donut may be due to a misalignment of the phase plate or a crooked placement of the sample. In order to capture a high quality STED image the minimum of the PSF of the STED laser must be aligned with the maximum of the PSF of the excitation laser. A plot profile is drawn for the two PSFs in both the x- and y-direction in order to see if the criteria mentioned above is achieved (Figure 15A, B). The resulting graphs shows that this is the case meaning that the alignment of the lasers was successful. The PSFs in the xz-direction can be seen in Appendix 3, Figure A3.1.

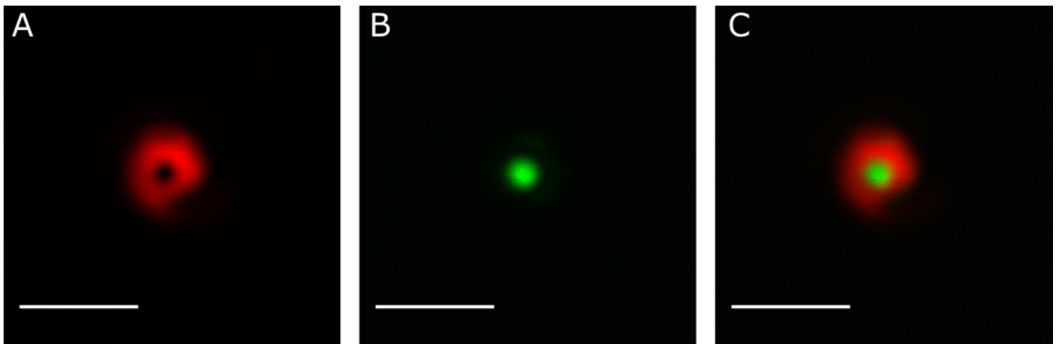

Figure 14: The reflected light of the STED and excitation laser in the Leica system viewed using gold nanoparticles. A) The PSF of the STED laser B) The PSF of the excitation laser C) The two PSFs combined. Scalebar is 1 µm

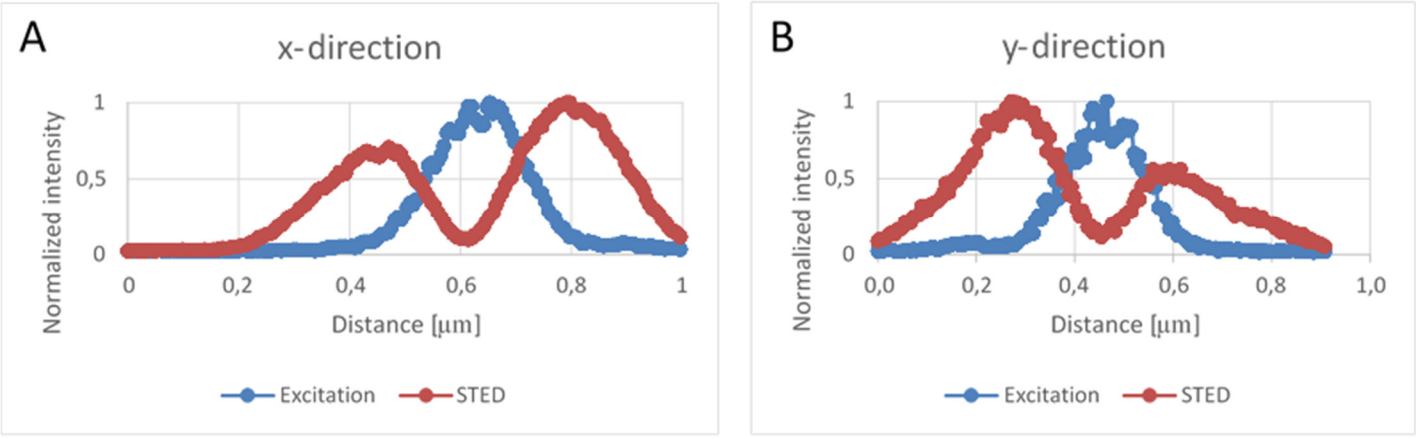

Figure 15: Plot profiles showing the normalized intensity as a function of the distance [µm] created over the PSFs of the STED and excitation laser in the x- and y-direction. A) Plot profile in the x-direction for Figure 14A) (red) and 14B) (blue) B) Plot profile in the y-direction for Figure 14A) (red) and 14B) (blue)

In order to show that the significantly enhanced resolution is dependent on the intensity of the STED laser an experiment is performed with fluorescent beads of different sizes: 20, 25 and 47 nm in diameter. A sample with individual separated beads but still a high bead density was sought. It was found that the optimum bead dilution for the 25 and 47 nm beads was 1:5000 and for the 20 nm beads the optimum bead dilution was 1:50.000. These dilutions will therefore be the ones examined further. For each bead size images were captured with an increasing intensity of the STED laser from 0 to 100 % of the STED laser operated at 70 % of its maximum power. At 100 % this corresponds to 1050 mW laser output. However the power delivered is much lower at the sample. Thereafter the diameter of 5 beads in each image is measured manually by creating a plot profile across a bead. The plot profiles were then, fitted with a Gaussian curve and the full width half maximum (FWHM) of the curves were calculated. The FWHM represents the measured diameter of the image of the bead. These are then plotted as a function of the STED intensity as well as the average diameters (Figure 16). In the resulting graph equation (2.7) is also plotted in order to compare the experimental results with the theoretical expectancy. The saturation level $\frac{I_{STED}}{I_s}$ for I_{STED}= 100%, has been

set to 40 as this has been seen to fit with experimental results [31], λ is the wavelength of the STED laser which in the Leica system is 592 nm and last the numerical aperture, NA of the system is 1,4. If one calculates equation (2.7) with these factors one may achieve a theoretical optimal resolution of approximately 30 nm.

The fluorescent beads with the diameter of 25 and 47 nm are from the same manufacturer and these beads exhibit similar tendencies. As expected all beads exhibit a measured diameter of approximately 200 nm when the STED intensity is 0 % which confirms (2.5). Afterwards the measured size of the beads and hence the resolution improves exponentially until it reaches a constant at about 30 nm which is consistent with (2.7). For the beads of 25 nm it is observed that the microscope achieves its optimum resolution as the experimental results match the theoretical result (Figure 16). For the 47 nm (Appendix 3, Figure A3.2) beads the microscope was also able to resolve the size of these beads. From this sample it cannot be said whether the microscope can achieve a better resolution as smaller samples are not present.

The last sample of beads with a diameter of 20 nm (Appendix 3, Figure A3.3) show the same tendency with a decreasing diameter as the STED intensity increases until it reaches a constant, but for this sample the size does not decrease at the expected rate. A resolution of about 50 nm is reached at 100 % STED intensity meaning the rate difference does not appear to be due to fluorescence leaking as this would have limited the resolution at a definite size. It may therefore be due to the dye not being suitable for STED imaging. This could be due to Anti-Stokes excitation of the dye with the STED depletion laser, low STED efficiency or contributions from components with short lifetimes.

In summery we can see that although the shape of the STED laser was suboptimal it was still possible to achieve a resolution down to 30nm.

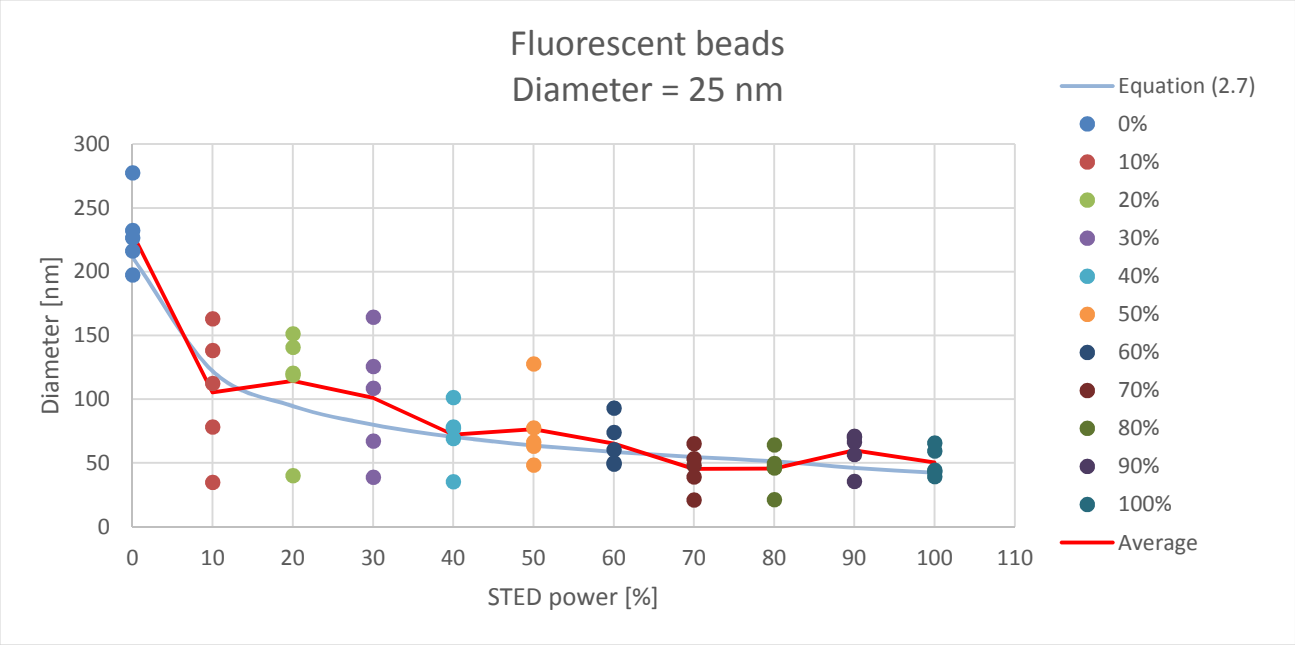

Figure 16: The diameter [nm] of 25 nm fluorescent beads as a function of the STED intensity [%]. For each STED intensity 5 bead diameter measurements are made and plotted. The average of the diameters is also plotted. Equation (2.7) is plotted with the following values: $\frac{I_{STED}}{I_S}$ =40 for I_{STED}=100%, λ=592 nm and NA=1,4.

3.2.2 Structure of human skin

It is now of interest to apply confocal and STED microscopy in order to study the structure of the epidermis. Preliminary experiments were performed in order to distinguish the optimal DMSO concentration in which dyes should be dissolved in to achieve the highest amount of labeling of the entire epidermis.

TopFluor DPPE

The first fluorescent dye tested was TopFluor DPPE (Appendix 2, Table 1) dissolved in the following DMSO concentrations in PBS: 0, 5, 10, 20, 30, 50, 60, 70, 85 and 100 %. This fluorescent dye is an amphiphilic molecule and has its fluorescent marker placed on the hydrophobic tale of the lipid molecule. Due to its small hydrophilic head group this makes it a highly hydrophobic molecule. It is therefore expected to pass through the SC via the intercellular lipid matrix but it may have difficulty doing so due to the size of the molecule. As mentioned earlier DMSO acts as a transport enhancer which is concentration dependent, and therefore it is expected to see a higher amount of labeling especially at a DMSO concentration above 60 %. [17] For each DMSO concentration an image in the xz-direction was captured in order to determine the amount and depth of sample labeling. From Figure 17A to 17E it is observed for the concentrations of DMSO from 0 to 30 % that the labeling of the SC, SG or SB

remains unchanged throughout these concentrations and that the labeling of the SC is not sufficient as only about 10-25% of the sample is labeled. At a concentration of 50 % DMSO an increased amount of labeled SC is observed and at a 100 % the highest amount of labeling is achieved where about 40 % of the sample is labeled. The samples labeled with 70 and 85 % DMSO (Figure 17H and 17I) also exhibit the same tendency i.e. the amount of labeling increases with an increasing DMSO concentration. At 60 % DMSO poor labeling is seen which is most likely due to an incorrect sample preparation. Although a high percentage of the sample is labeled (54%) at a concentration of 85 % DMSO the labeling is more evident in the sample labeled in 100 % DMSO as the dye concentration is higher in the SC.

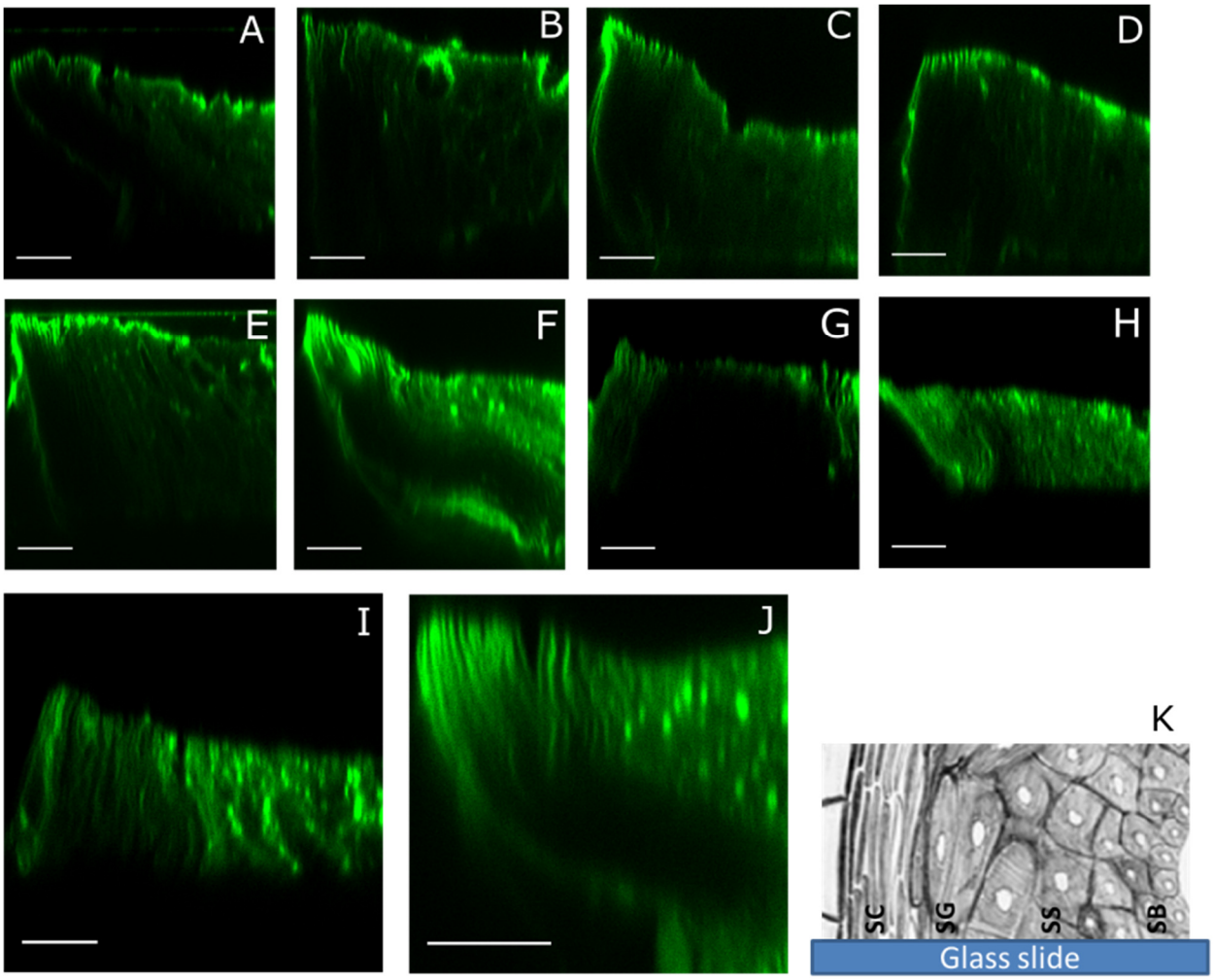

Figure 17: Confocal images in the xz-direction of skin samples labeled with the hydrophobic dye TopFluor DPPE dissolved in different DMSO concentrations. In each image SC is visible on the left and the underlying layers towards the right. Samples G-I are cut in 20 µm slices. Remaining are cut in 30 µm slices. A) 0% DMSO B) 5 % DMSO C) 10% DMSO D) 20 % DMSO E) 30% DMSO F) 50% DMSO G) 60 % DMSO H) 70 % DMSO I) 85 % DMSO J) 100% DMSO K) Sketch of the placement of the skin samples in A-J . Scalebar is 10 µm.

ATTO 488 DPPE

Another amphiphilic fluorescent dye ATTO 488 DPPE (Appendix 2, Table 2) was also tested. This molecule has a quite large fluorescent marker placed on the hydrophilic head group. Due to the increased size of the head group it is expected to have a lower permeability through SC compared to TopFluor DPPE. But due to its hydrophobicity it is expected to use the pass through the intercellular lipid matrix in the SC. The same experiment with different DMSO concentrations was performed. A similar behavior as that found with the TopFluor DPPE was expected. The DMSO concentrations in this experiment were 0, 5, 30 and 100 %. As seen in Figure 18A and 18B at 0 and 5 % DMSO there is almost no labeling of the SC while the underlying layers are labeled quite well. The reason for this may be that the increased size of the hydrophilic head group making it more difficult to penetrate the SC or that it has a low partition coefficient for the tightly packed lipids in the SC. At 30 and 100 % DMSO a higher amount of the SC is labeled but a lower labeling efficiency is seen in the underlying layers. In this experiment DMSO did not show the expected effect as the labeling becomes poorer as the DMSO concentration rises. This may be caused by ATTO 488 DPPE not participating into the skin and having a greater affinity for DMSO than the sample. So when the sample is washed most of the dye will be washed out along with the DMSO solution.

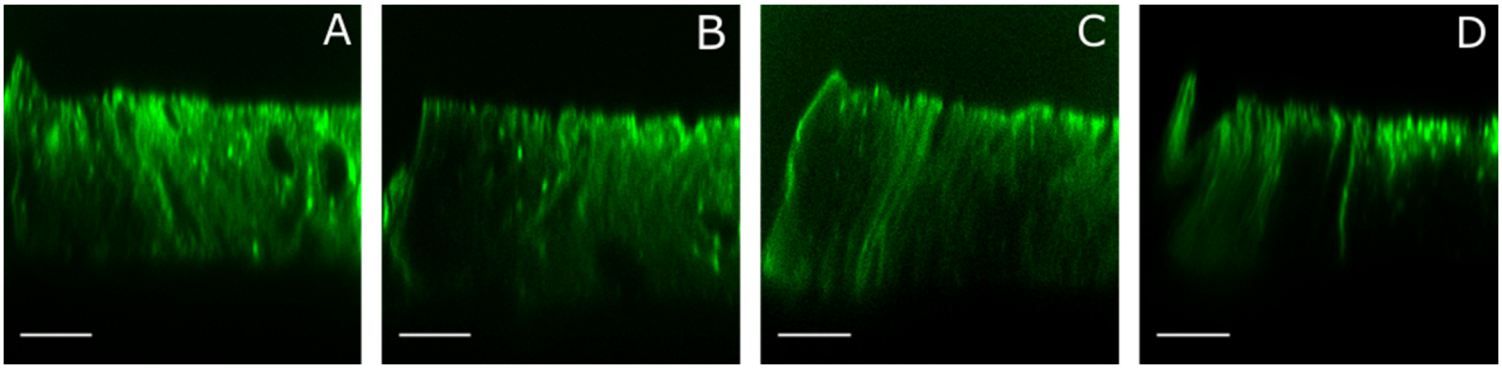

Figure 18: Confocal images in the xz-direction of skin samples labeled with the hydrophobic dye ATTO 488 DPPE dissolved in different DMSO concentrations. In each image SC is visible on the left and the underlying layers towards the right. The samples are all cut in 20 µm slices. A) 0% DMSO B) 5 % DMSO C) 30% DMSO D) 100 % DMSO. Scalebar is 10 µm

Sample swelling and sectioning thickness

In the experiment for determining the DMSO concentration needed to achieve the best labeling of the SC with the fluorescent dye TopFluor 488 DPPE (Figure 17) the samples were sliced in 30 µm slices. It is observed in Figure 17 that the SC has a tendency to swell due to the high level of hydration. Since the fluorescent dye does not penetrate the entire sample it becomes problematic to visualize all the layers of the epidermis simultaneously as the layers are not labeled at the same plane. An experiment is therefore performed in order to determine whether or not thinner slices will optimize the labeling. Samples were sliced in 10 and 30 µm

and each labeled with 5, 30 and 100 % DMSO. Again images in the xz-direction were captured in order to determine the amount of labeling and swelling. In general it is observed that the SC does not swell quite as much (Figure 19A to 19C) with a slice thickness of 10 µm proportional to the 30 µm. However the structures of the epidermis do become less apparent. With a concentration of 5 % DMSO the amount of labeling of the sample is similar for both 10 and 30 µm. At 30 % DMSO almost none of the sample is labeled for both 10 and 30 µm which may due to incorrect sample preparation. At 100 % DMSO both samples show a high amount of labeling of the SC and the dye has labeled the entire sample in the 10 µm sample as expected. In order to achieve minimal swelling of the sample while still preserving the structures of the skin samples of 20 µm in thickness were found to be the best compromise.

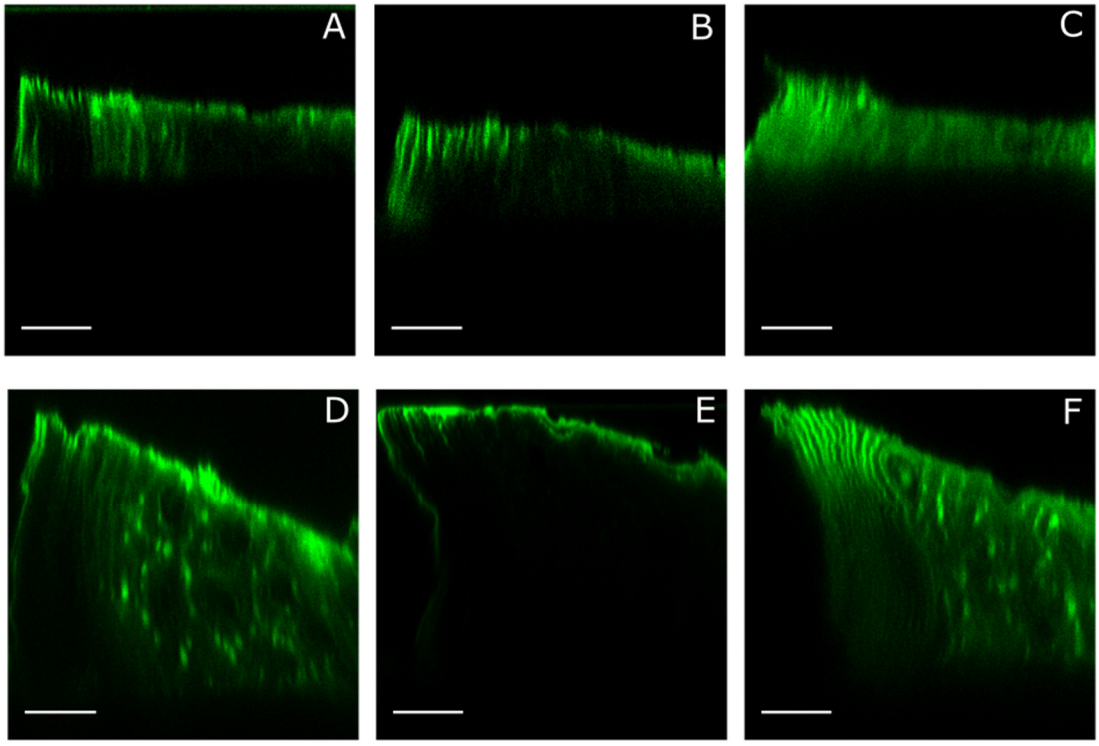

Figure 19: Confocal images in the xz-direction of skin samples labeled with the hydrophobic dye TopFluor DPPE dissolved in different DMSO concentrations. In each image SC is visible on the left and the underlying layers towards the right. Samples A) to C) are cut in 10 µm slice while samples D) to F) are cut in 30 µm slices. A) 0% DMSO B) 30 % DMSO C) 100% DMSO D) 0 % DMSO E) 30% DMSO F) 100% DMSO. Scalebar is 10 µm

Imaging the intercellular lipids in the SC

From the experiments above the following conclusions can be drawn and used in the subsequent experiments. In order to achieve the highest amount of labeling TopFluor DPPE must be dissolved in 100 % DMSO while ATTO 488 DPPE must be dissolved in buffer with 0 % DMSO. With these conditions an experiment was performed were the sample was labeled with TopFluor DPPE (DMSO) overnight and then ATTO 488 DPPE (PBS) overnight. It is

desired to take a closer look at the general structure of the skin via labeling of the hydrophobic regions. In the SC it is expected to observe labeling of the intercellular lipid matrix while in the underlying layers it is expected to see labeling of the lipid membranes of the cells. Confocal and STED images were taken and both of these were deconvolved using Huygens (Figure 20).

A plot profile of both images is then created by drawing a line at the same place in both images. The resulting plot profiles are then plotted in the same graph in order to compare. In the confocal image of the SC (Figure 20D) the width of intercellular lipids is measured. The widths of each of these lipid sheets are measured to be at around 200 nm (Figure 21, blue) i.e. the smallest size measurable in the system due to diffraction. In the STED image the same lipid sheets are also measured (Figure 20C). Here a decreased width is observed to around 100 nm (Figure 21, red). Structures that in the confocal image gave rise a single peak in the plot profile now in the STED image appear with the hint of a shoulder as well as several small peaks in between the larger peaks which may indicate structures in the SC that were not resolvable in the confocal image.

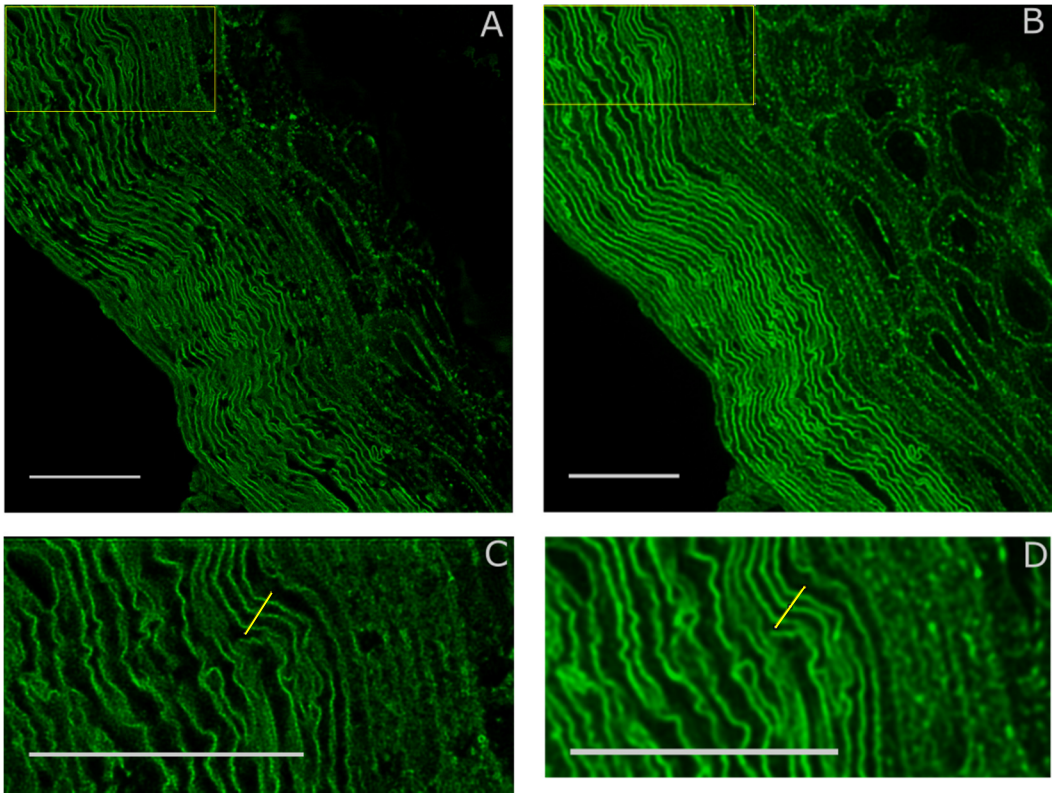

Figure 20: Confocal and STED images of the same area of the epidermis where the sample is labeled with the hydrophobic dyes TopFluor DPPE and ATTO 488 DPPE. A) STED image of the epidermis. SC to the left. C) Zoom of the marked area in A). B) Confocal image of the epidermis. SC to the left. D) Zoom of the marked area in B). Scalebar is 10 µm.

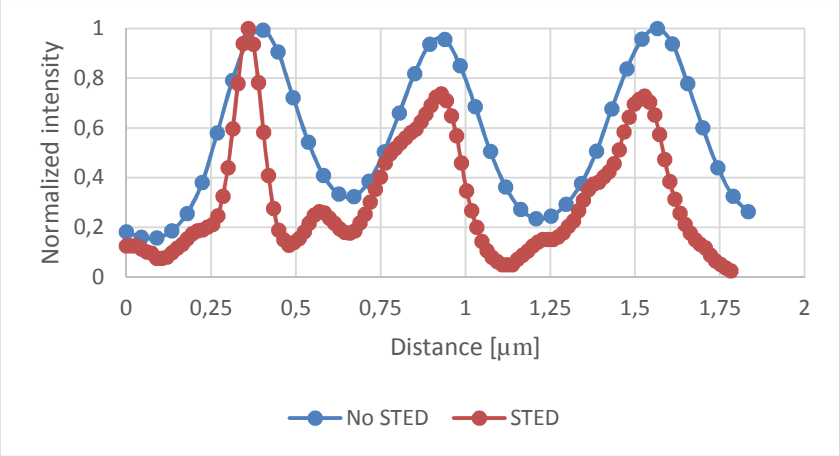

Figure 21: Plot profile showing the normalized intensity as a function of the distance [µm] created along the drawn line in Figure 20 C) (red) and D) (blue).

Imaging hydrophilic molecules in the epidermis

It is also of interest to look at the structure of the skin via labeling of the hydrophilic regions. Rhodamin B (Appendix 2, Table 3) is a small hydrophilic molecule. Due to its small size one may expect it to have easier access to the corneocytes and therefore penetrate the SC through the intracellular pathway. Also Rhodamin B has been observed to label keratin [32] which may cause the dye to label the keratin inside the corneocytes. Another option is that the dye passes through the SC using the aqueous regions in the lipid matrix ergo via the intercellular pathway (Figure 3). In the underlying layers of the epidermis it is expected to see a labeling of the cell cytoplasm. Due to the fact that the used Leica system only has a STED laser at 592 nm STED images could not be obtained for Rhodamin B as this is in the excitation region of this dye. It would therefore excite the molecules and not deplete them. Therefore only confocal images were taken. In the following images (Figure 22) no structured labeling of the SC is observed. On the other hand the labeling of SC appears to be smeared throughout the entire SC with only a structured labeling where the corneocytes are detaching from one another. This is thought to be caused during sample preparation. It may therefore appear as if Rhodamin B labels the corneocytes as well as the intercellular lipid matrix. In the SG the cellular structures are becoming more visible as Rhodamin B labels the cell cytoplasm. In the SS and towards the SB the cell structures become even more visible and a characterizing structure in between the cells is observed, looking like train tracks. These tracks may be the cellular keratin associated with desmosomes as Rhodamin B labels keratin[33]. The experiment of labeling with Rhodamin B was performed in two ways: with and without washing (step 6) in protocol (1)). It was expected that Rhodamin B might partition to the PBS buffer rather than the sample if this was washed and the dye concentration would therefore be considerately lower. The washed sample did show lower dye concentration as expected (Figure 22). In the non-washed sample the keratin structures between the cells become less

visible (Figure 23). In general when looking at the images from these experiments no major structural difference are observed between the two procedures.

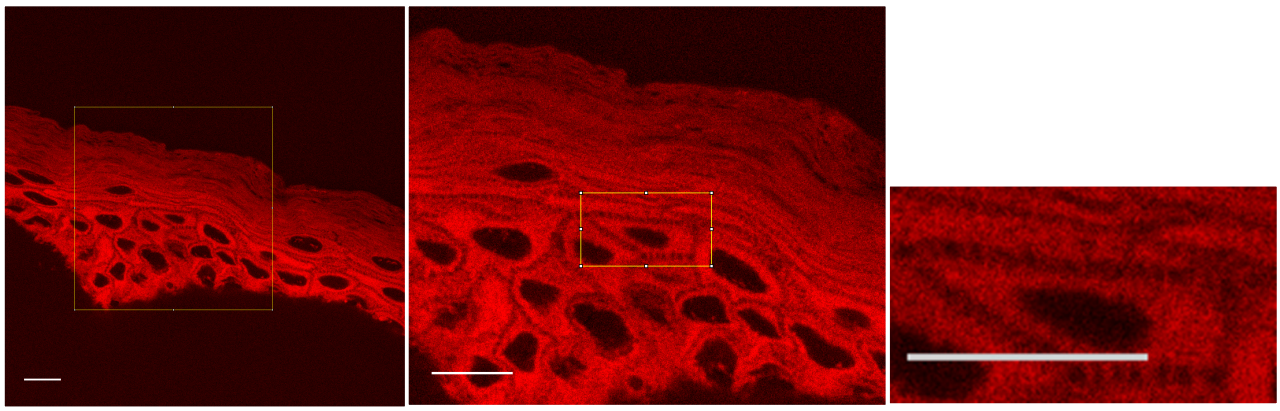

Figure 22: Confocal images of the epidermis where the sample is labeled with the hydrophobic dye Rhodamin B and subsequent zooms of the marked areas on the previous image. On the first two images SC is visible at the top. The last image shows a zoom of a single cell in SS. This sample was washed (step 6) in protocol (1)). Scalebar is 10 µm.

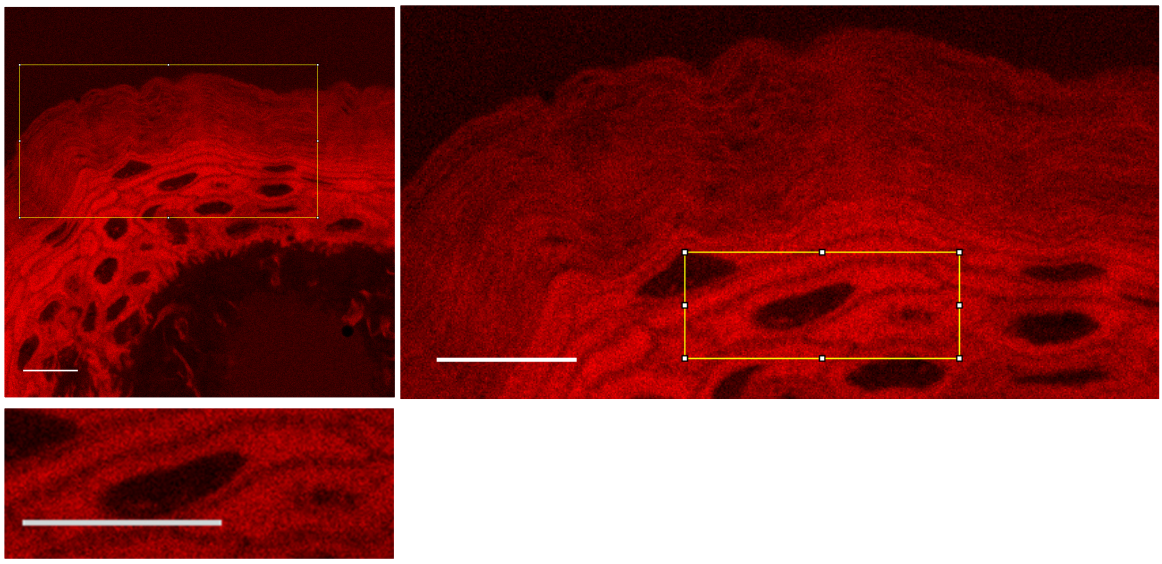

Figure 23: Confocal images of the epidermis where the sample is labeled with the hydrophobic dye Rhodamin B and subsequent zooms of the marked areas on the previous image. On the first two images SC is visible at the top. The last image shows a zoom of a single cell in SS. This sample has not been washed (step 6) in protocol (1)). Scalebar is 10 µm

Because the labeling of the SC appeared smeared when labeling with Rhodamin B, which may be due to affinity for keratin, another hydrophilic dye was tested: ATTO 647 N (Appendix 2, Table 4). This dye is larger than Rhodamin B and it is therefore expected to have more difficulty penetrating the corneocytes. This may therefore inhibit both the intra- and intercellular pathway. Also this dye has not been shown to label keratin so therefore labeling of the corneocytes is not expected in the same degree as for Rhodamin B. However it is still expected to show the same characteristic labeling of the underlying layers as Rhodamin B with exception of the keratin structures. In the images (Figure 24) a smeared labeling of the SC is again observed which again implies labeling of both corneocytes and the intercellular lipid matrix. In the underlying layers the similar behavior as for Rhodamin B is observed, thus a labeling of the cell cytoplasm but no keratin structures are observed. The experiment with ATTO 647N was also performed in two ways as with Rhodamin B. When comparing the two procedures no specific difference is observed (Figure 24).

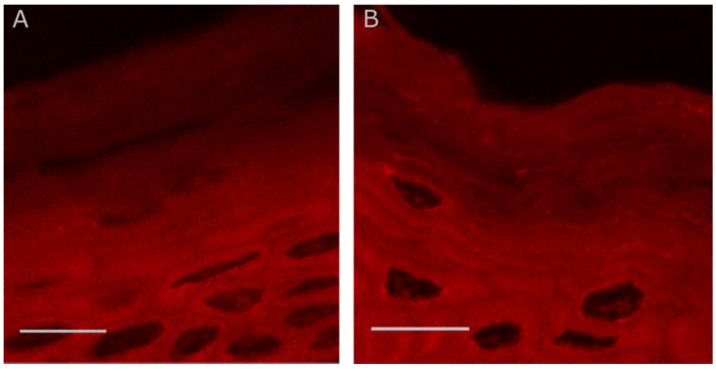

Figure 24: Confocal images of the epidermis where the sample is labeled with the hydrophilic dye ATTO 647 N. SC can be seen on top on both images. A) The sample has been washed (step 6) in protocol (1)) B) The sample has not been washed. Scalebar is 10 µm

As it is not possible to capture STED images of the Rhodamin B dye it is therefore of interest to find a hydrophilic dye that can enable STED images to be captured. Such a dye may be

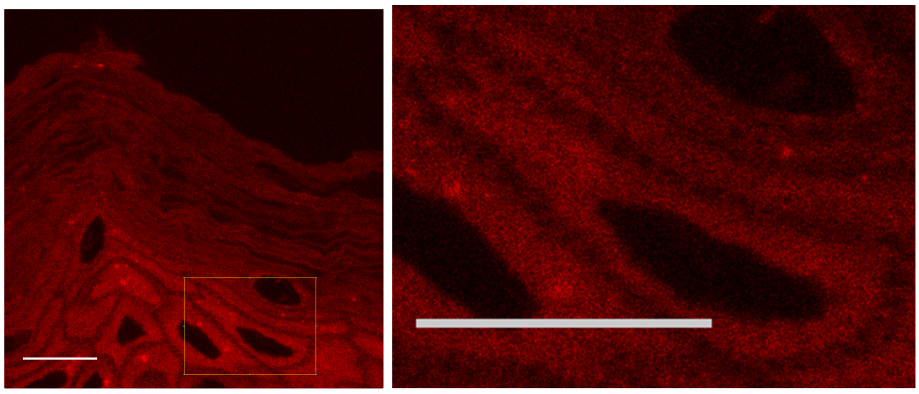

Figure 25: Confocal image of the epidermis where the sample is first labeled with the hydrophilic dye Abberier Star 440 SX. The second image is a zoom of the marked area in the first image. To the left SC can be seen on top. This sample has been washed (step 6) in protocol (1)). Scalebar is 10 µm.

Aberior Star 440 SX (Appendix 2, Table 5). Samples labeled with this dye were therefore made and again in two ways: with and without washing. (step 6) in protocol (1)). These samples are visualized using confocal microscopy (Figure 25 and 26). In both cases the dye labels the cell cytoplasm in the SB as expected. The structures seen between the cells in the SB are however not as clear as in the sample that has not been washed. Another problem in the non-washed sample is that the dye labels the coverslip which complicates the location of the SC. In the washed sample this is not an issue and therefore the focus will be on this sample. As mentioned earlier some structure is visible between the cells in the SB that is similar to the structures observed in Rhodamin B samples. This indicates that Abberior Star 440 SX also labels keratin. In the SC clear structures can be seen but it is not possible to distinguish

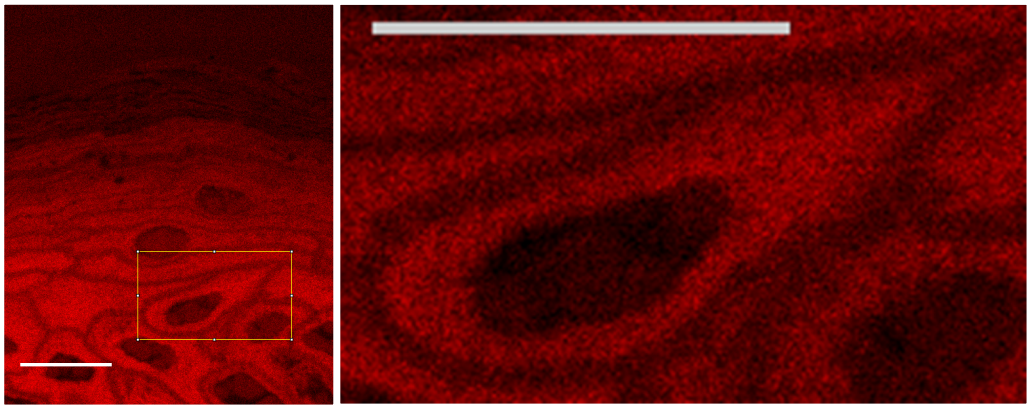

Figure 26: Confocal image of the epidermis where the sample is labeled with the hydrophilic dye Abberior Star 440 SX. In the first image SC can be seen on top. The second image shows a zoom of a single cell from the marked area in the previous image. This sample has been washed (step 6) in protocol (1)). Scalebar is 10 µm.

whether the corneocytes or the intercellular lipid matrix has been labeled. But due to the labeling of keratin in the underlying layers this points to labeling of the corneocytes. However the structure could also resemble a SC structure where the corneocytes detach from one another.

3.2.3 Transport pathways through the skin

Samples labeled with both hydrophilic and hydrophobic dyes are used in order to determine their pathway and placement through the epidermis. As mentioned earlier the hydrophobic dye TopFluor DPPE exhibits a better labeling of the SC when dissolved in 100% DMSO while Rhodamin B is dissolved in 100 % PBS buffer. It is therefore of importance to look at the effect of DMSO when labeling with Rhodamin B.

A sample was first labeled with DMSO overnight and afterwards with Rhodamin B (Figure 27). It is evident that the characteristic keratin structures are no longer visible in this sample. Simultaneously the labeling of the SC and the underlying layers has become even more smeared which implies that DMSO has a prolonged effect on the epidermis making penetration easier throughout the entire epidermis. The experiment is then performed with the sample being labeled with Rhodamin B overnight and afterwards with DMSO (Figure 28). In this case it is observed that the labeling of the outermost part of SC has become almost none existing and only the innermost part of SC is labeled. In the SC there are fewer hydrophilic regions available. Rhodamin B may therefore have a greater affinity for DMSO than the sample and will therefore be washed out in this region. As the underlying layers of the epidermis contain large hydrophilic regions it is more favorable for Rhodamin B to remain within these. The keratin structures in the underlying layers are now slightly visible but the labeling still appears more smeared throughout the sample in comparison to the samples without DMSO (Figure 22 and 23).

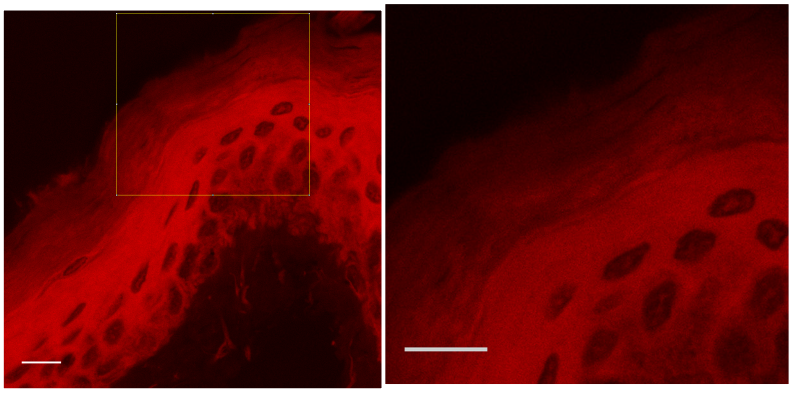

Figure 27: Confocal image of the epidermis where the sample is first labeled with DMSO overnight and then with the hydrophilic dye Rhodamin B. The second image is a zoom of the marked area in the first image. On both images SC can be seen on top. Scalebar is 10 µm.

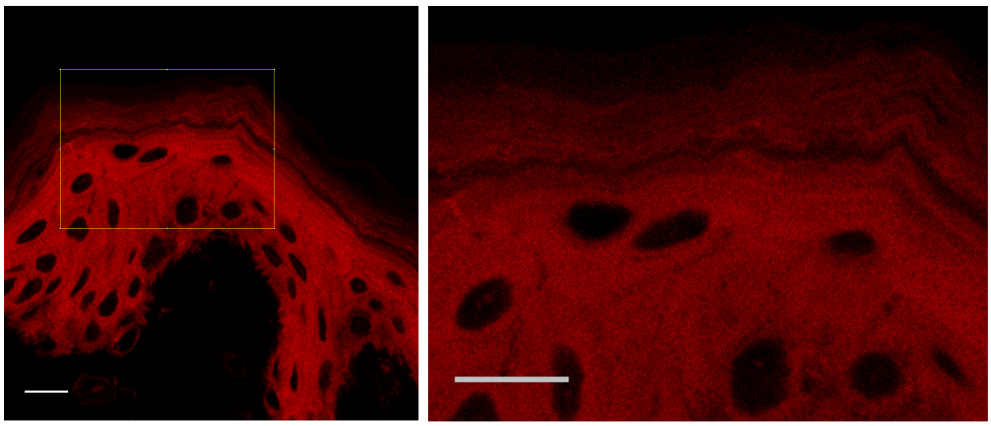

Figure 28: Confocal image of the epidermis where the sample is first labeled with the hydrophilic dye Rhodamin B overnight and then with DMSO. The second image is a zoom of the marked area in the first image. On both images SC can be seen on top. Scalebar is 10 µm.

It is expected that the placement of Rhodamin B in the lower part of the SC and SG will be more distinct if the sample is labeled as in Figure 27. However if the outer most part of the SC is of interest labeling as in Figure 28 is optimal. From these images it is not conclusive which sample preparation is optimal and both methods will therefore be used in subsequent experiments.

To investigate the transport pathway through the skin experiments are performed where the labeling dye is placed upon intact skin i.e. before slicing. This experiment is first performed with the hydrophobic dye TopFluor DPPE. From the image it can be seen that the dye does not penetrate the SC (Appendix 3, Figure A3.4). The experiment is then performed with the hydrophobic dye Rhodamin B (Figure 29A). A clear labeling of the entire skin sample is observe however the labeling of the SC is once again smeared as seen in previous experiment. The molecules compared are respectively hydrophilic and hydrophilic. This experiment suggests that the molecular weight of a molecule in the partition coefficient is an important part of diffusion through the skin as the smaller dye can penetrate the entire epidermis and the larger dye cannot. The observation that molecules below 500 Da usually penetrate the skin is referred to as the "500 Dalton rule". [34] However the different affinities of the molecules make it difficult to conclude from this experiment whether the size of the molecule is the all-determining factor in diffusion as the possibility to enter the skin also depends on the polarity and lipophilicity of the applied molecule.

In Figure 17 it can be seen that the dye applied after slicing does not penetrate through the entire sample. This shows that the skin still maintains its barrier function even when sliced. One can therefore investigate not only the placement of a dye but also the transport pathway when labeling after slicing. Samples were prepared with Rhodamin B applied on intact skin i.e. before slicing and TopFluor DPPE and ATTO 488 DPPE applied after slicing. In this experiment it is hoped to see whether or not the different dyes with different affinities will appear at different parts of the SC. Because of the hydrophobicity of TopFluor DPPE and ATTO 488 DPPE it is expected for this dye to penetrate the SC through the intercellular lipid matrix. For Rhodamin B there are more possibilities. As mentioned earlier one of these is that due to the dyes smaller size and affinity it could pass easier through the corneocytes and therefore use the intracellular pathway but in order to do so there must be a certain amount of unbound water available in these, which literature suggests is limited. [19] Rhodamin B does however label keratin so labeling may be observed in the corneocytes and the dye therefore could use the intracellular pathway. The last option is that dye passes through the intercellular lipid

matrix but in the aqueous region as seen in Figure 3. In Figure 29 the live cells in the SS are visible and the cellular nucleus can be distinguished. It can be seen that the cells flatten throughout the SS, SG and SC as they differentiate. The placement of the two dyes in the sample throughout the SC is then examined. This is done by creating a plot profile along the lines shown in Figure 29A and 29B. From the plot profile (Figure 30) it appears that Rhodamin B labels the intercellular lipid matrix. Many of the maxima for hydrophobic dye correspond to maxima for the hydrophilic dye. Some of these corresponding maxima also appear to be shifted from one another which may be due to different filter settings or the image being recorded with different colors in a non-acromatic system. In this experiment Rhodamin B was dissolved in 100 % DMSO and as it was mentioned earlier DMSO acts as transport enhancer by creating larger hydration shells surrounding the lipid head groups making the aqueous regions in the intercellular lipid matrix larger. Because Rhodamin B has previously shown a tendency to label keratin and yet labels the intercellular lipid matrix when applied before slicing and dissolved in DMSO this points to DMSO making the intercellular pathway more accessible.

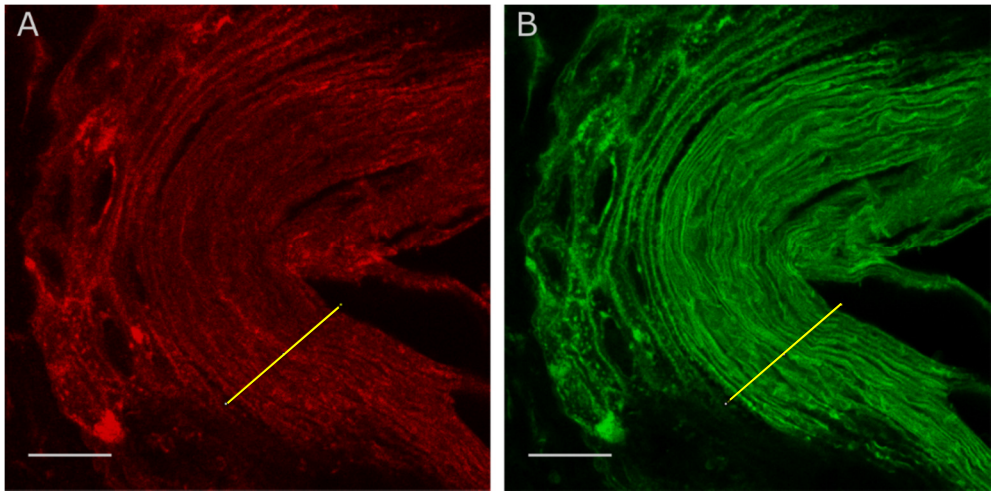

Figure 29: Confocal images of the epidermis where the sample was first labeled with Rhodamin B on intact skin i.e. before slicing (BS) and then with ATTO 488 DPPE and TopFluor DPPE on the sliced sample. On both images SC can be seen to the right. A) Confocal image of the epidermis labeled with Rhodamin B before slicing. B) Confocal image of the epidermis labeled with ATTO 488 DPPE and TopFluor DPPE after slicing. Scalebar is 10 µm.

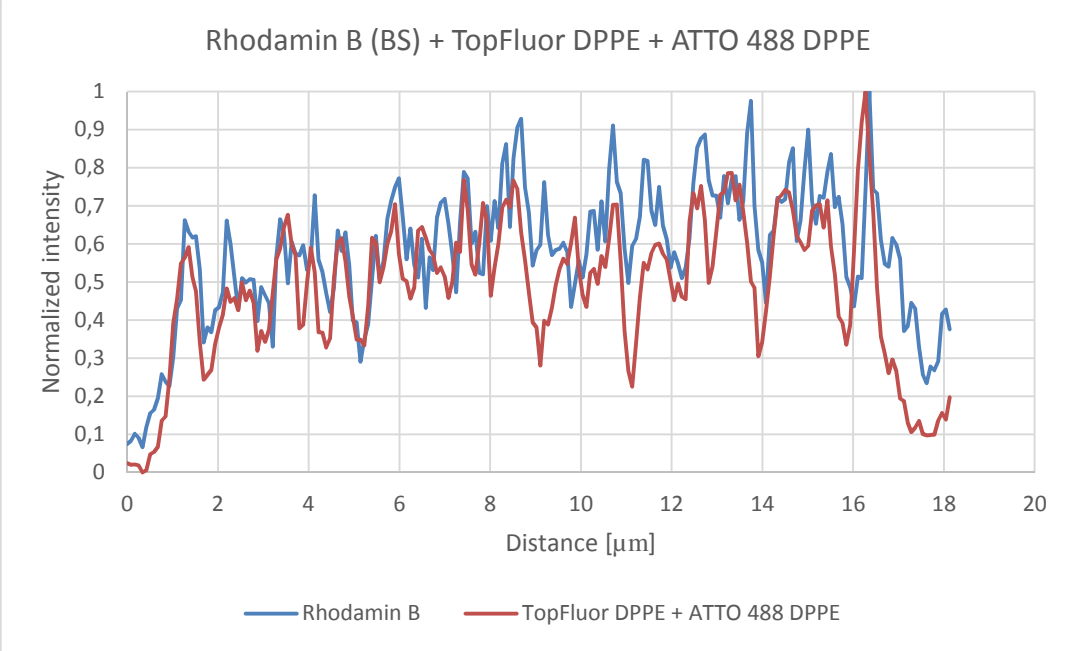

Figure 30: Plot profile showing the normalized intensity as a function of the distance [µm] created from tne drawn line in Figure 29A) (blue) and B) (red).

More experiments with the dyes Rhodamin B, TopFluor DPPE and ATTO 488 DPPE were performed where all the dyes were applied after slicing. The first experiment was performed with first applying Rhodamin B and ATTO 488 DPPE both dissolved in PBS to the sample overnight and then TopFluor DPPE dissolved in DMSO overnight. For Rhodamin B it is expected to see almost no labeling of the outermost part of SC as described earlier (Figure 28).

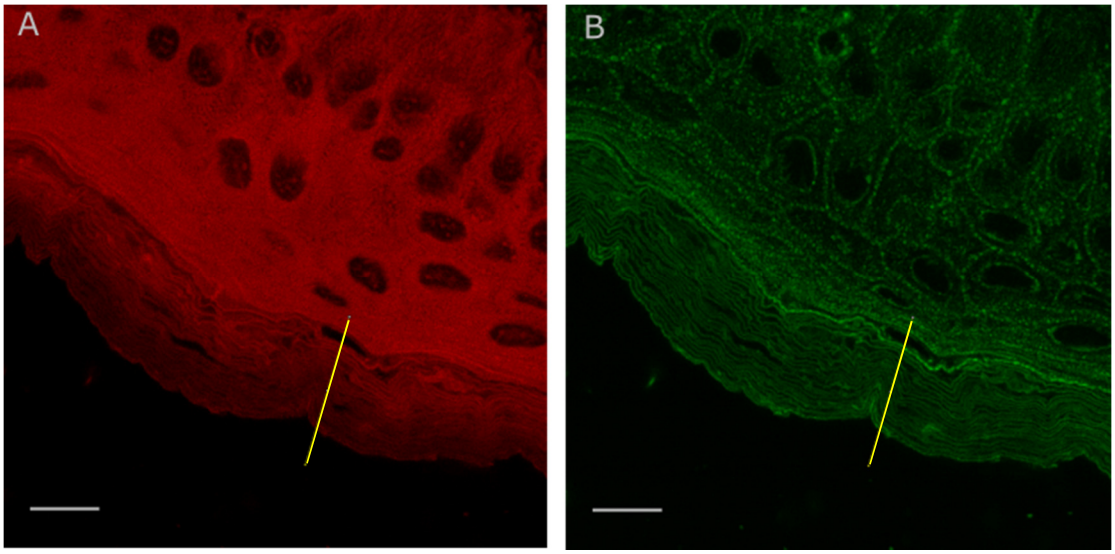

Figure 31: Confocal images of the epidermis where all dyes are applied to the sample after slicing. The sample is first labeled with Rhodamin B and ATTO 488 DPPE overnight and with TopFluor DPPE afterwards. On both images SC can be seen at the bottom. A) Confocal image of the epidermis labeled with Rhodamin B B) Confocal image of the epidermis labeled with ATTO 488 DPPE and TopFluor DPPE. Scalebar is 10 µm.

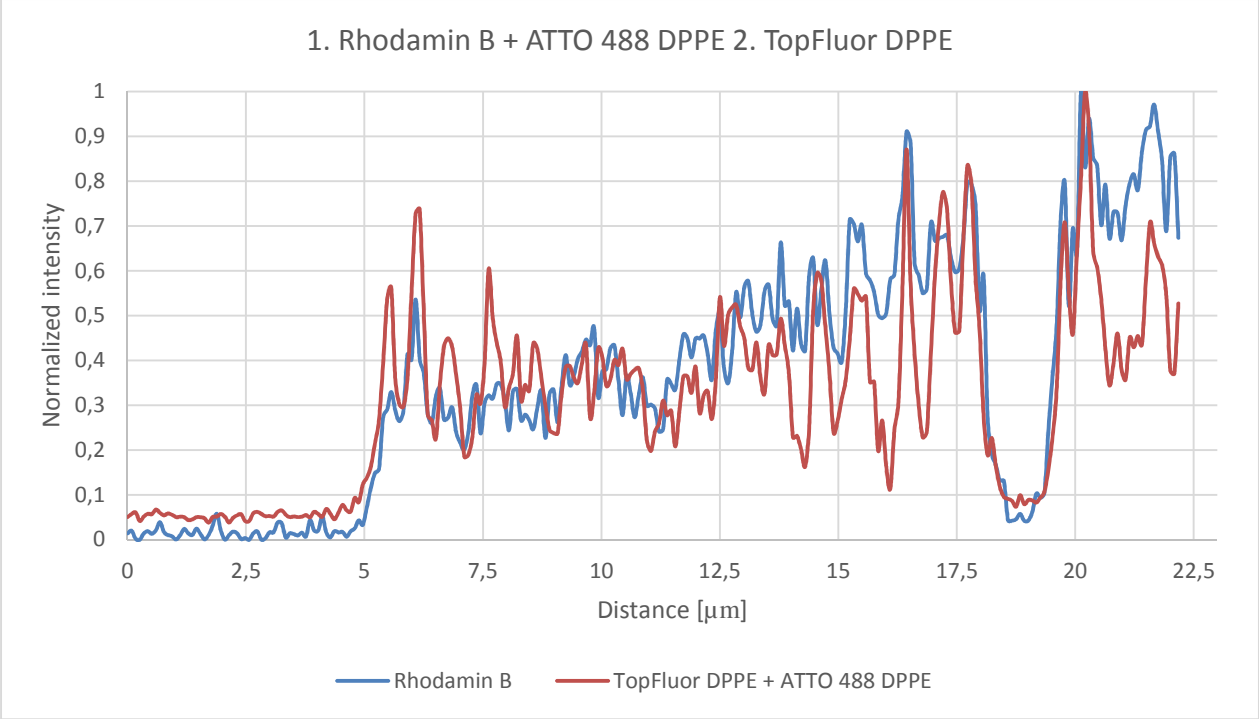

Figure 32: Plot profile with the normalized intensity as a function of the distance [µm] created from the drawn line in Figure 31A) (blue) and B) (red).

A plot profile is made along the drawn line in the SC (Figure 31A and 31B). The resulting graph (Figure 32) clearly shows that Rhodamin B does not label any clear structures in the SC as the plot shows many small peaks along SC. The plot for TopFluor DPPE and ATTO 488 DPPE shows a structured labeling of the SC. From these images it is therefore not possible to determine whether the two dye types use the same transport pathway through the skin or not. The same experiment is then performed where the sample first labeled with TopFluor DPPE (DMSO) overnight and then Rhodamin B (PBS) and ATTO 488 DPPE (PBS) overnight (Figure 33A and 33B). Here the labeling with Rhodamin B is expected to become smeared throughout the SC but yet still labeling the entire SC (Figure 27). The plot profile (Figure 34) shows the same tendency for Rhodamin B ergo a smeared labeling of SC. Thus it is not possible to determine whether the dyes use the same pathway through the skin or not from these images, however it is clear that Rhodamin B can be found inside the intracellular space of the corneocytes. This is in contrast to the lipophilic.

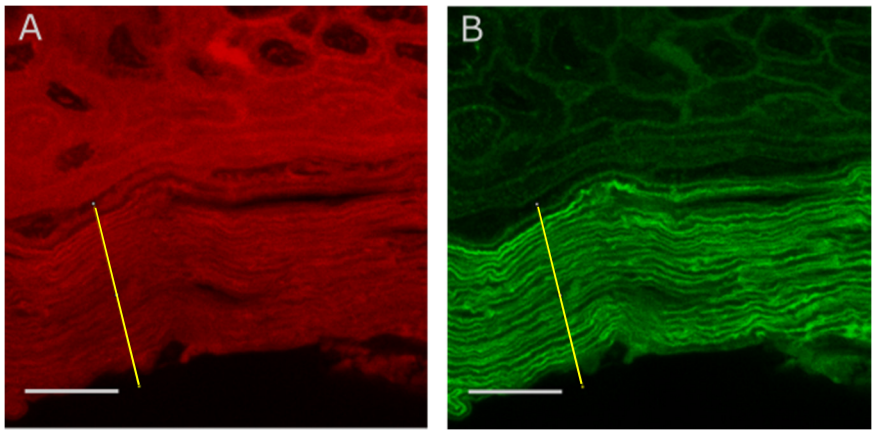

Figure 33: Confocal images of the epidermis where all dyes are applied to the sample after slicing. The sample is first labeled with TopFluor DPPE overnight and with Rhodamin B and ATTO 488 DPPE afterwards. On both images SC can be seen at the bottom. A) Confocal image of the epidermis labeled with Rhodamin B B) Confocal image of the epidermis labeled with ATTO 488 DPPE and TopFluor DPPE. Scalebar is 10 µm.

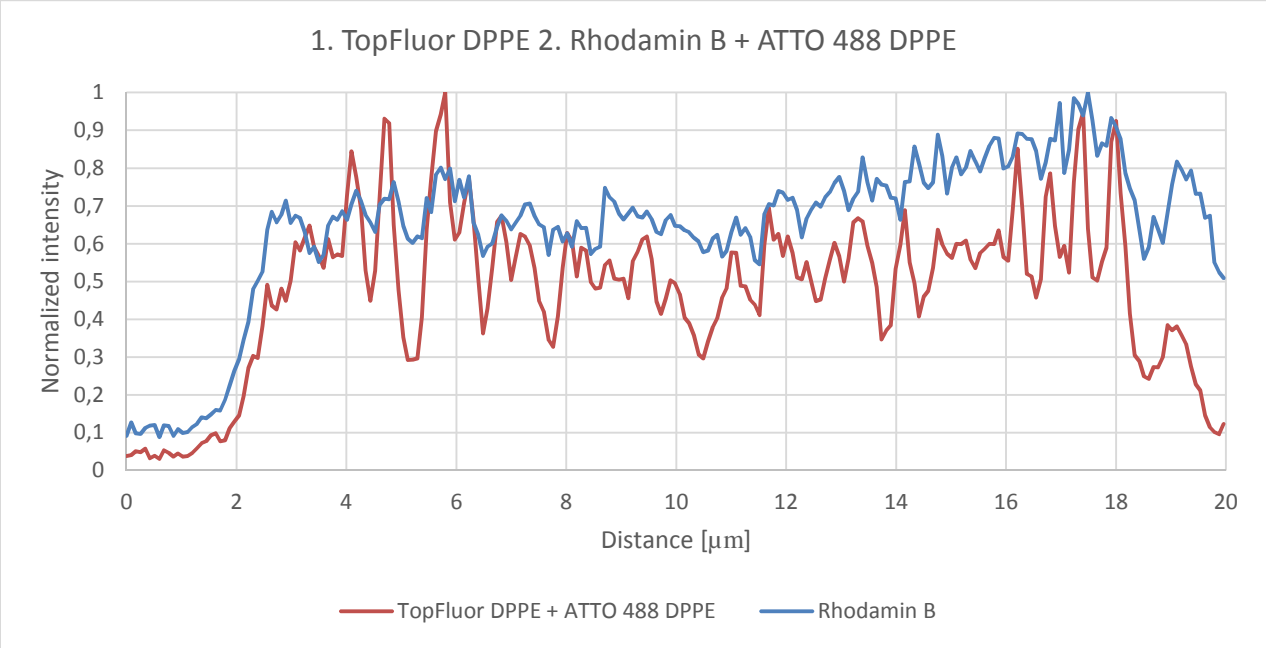

Figure 34: Plot profile with the normalized intensities as a function of the distance [µm] created from the drawn line in Figure 33A) (blue) and B) (red).

Abberior Star 440 SX

Another experiment was performed in order to determine the transport pathway through the skin with the hydrophilic dye Abberior Star 440 SX. For this dye it has been observed earlier that labeling of keratin occurs in the underlying layers of the epidermis. Therefore it is expected to see labeling of the corneocytes and therefore an indication of this dye using the intracellular pathway. The hydrophobic dyes in this experiment were TopFluor DPPE and ATTO 488 DPPE and these are expected to use the intercellular pathway through the skin. In this experiment both the hydrophilic and hydrophobic dyes were applied after slicing. During the previous and all following experiments with Abberior Star 440 SX an Argon laser was used as the excitation laser as this has the lowest available wavelength. It was not possible to

capture a STED image of this dye. In the following images the hydrophilic dye is recorded with confocal microscope while the hydrophobic dyes were recorded with STED. Both images are deconvolved (Figure 35A and 35B). On these images a plot profile (Figure 36) is created along the drawn line in order to determine the placement of the two dyes. The resulting plot profile shows that Abberior Star 440 SX labels structures of the SC as distinct peaks are visible which is also the case for the hydrophobic dyes. Also it can now be determined whether the two dyes use the same pathway through the skin or not. As seen on the plot profile the majority of the maxima for the hydrophilic dye correspond to a maximum for the hydrophobic dye. The hydrophobic dyes are recorded with STED so several new peaks are observed. These are not resolved in the hydrophilic plot profile but lie within the maxima of these. This suggest that the two dyes are mainly confined to the intercellular pathway.

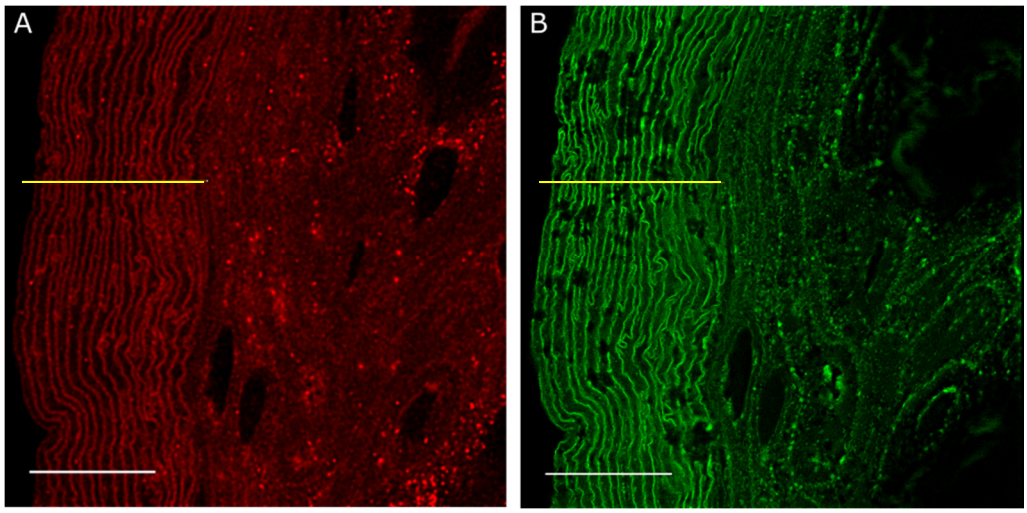

Figure 35: Confocal images of the epidermis where all dyes are applied to the sample after slicing. The sample is first labeled with with Abberior Star 440 SX and ATTO 488 DPPE overnight and with TopFluor DPPE afterwards. On both images SC can be seen to the left. A) Confocal image of the epidermis labeled with Abberior Star 440 SX B) STED image of the epidermis labeled with ATTO 488 DPPE and TopFluor DPPE. Scalebar is 10 µm

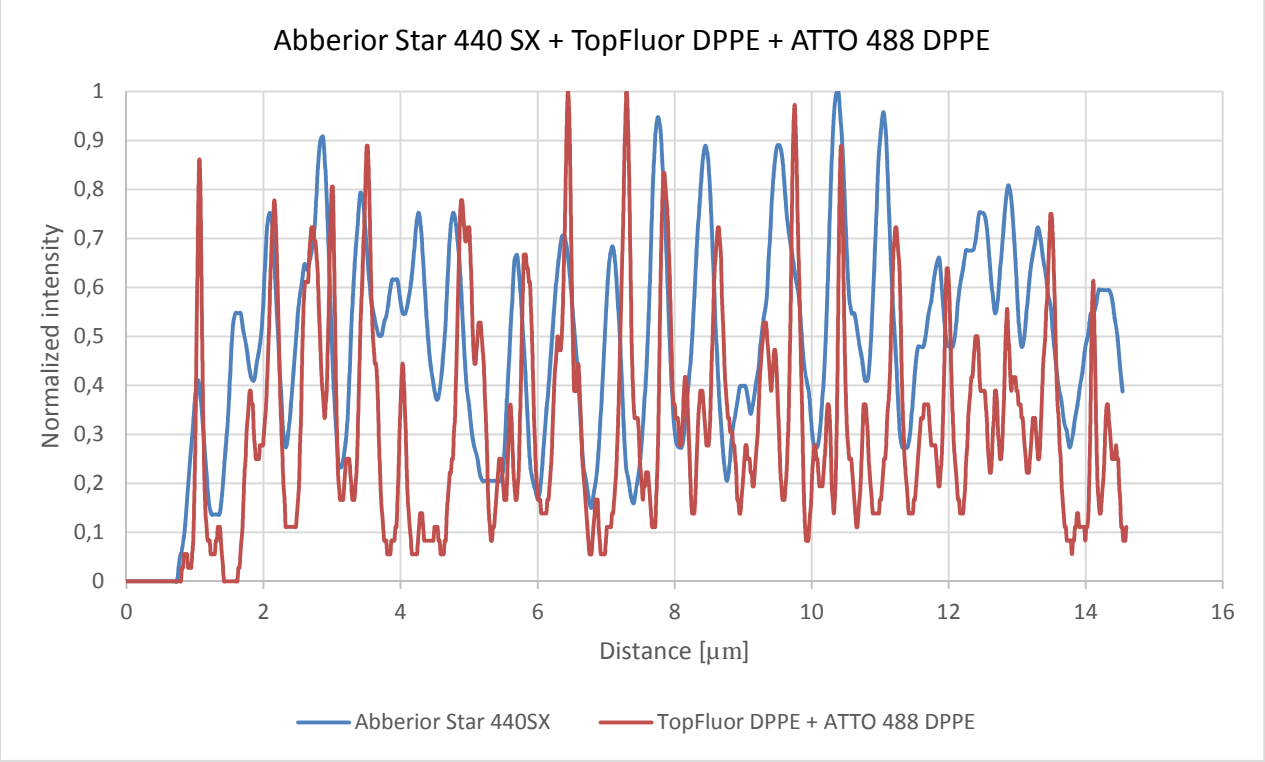

Figure 36: Plot profile with the normalized intensity as a function of the distance [µm] created from the drawn line in Figure 35A) (blue) and B) (red).

3.2.4 Antibody labeling

In order to examine specific structures in the epidermis the protein desmoplakin has been labeled through immunolabeling. Using the Leica system STED images were captured and thereafter deconvolved. As desmoplakin appear in pairs (Figure 2) it is expected to observe pairwise structures. The distance between the C-terminals of a pair of desmoplakins is said to be around 100 nm plus the width of the intercellular space. [15] It is also expected to observe a lower density of desmoplakin at the SC and higher in the SG, SS and SB. The resulting image is taken in the lower SG as almost no structures were observed in the SC as expected. The image (Figure 37) shows clear pairwise structures that lie opposite each other. The distance between these is measured by creating a plot profile over such a pair. The plot profile across the drawn line in the bottom image can be seen in Appendix 3, Figure A3.5. This is done on 3 pairs and the average distance between these was found to be around 160 nm. This corresponds to expected value meaning that the width of the intercellular space in around 50-60 nm.

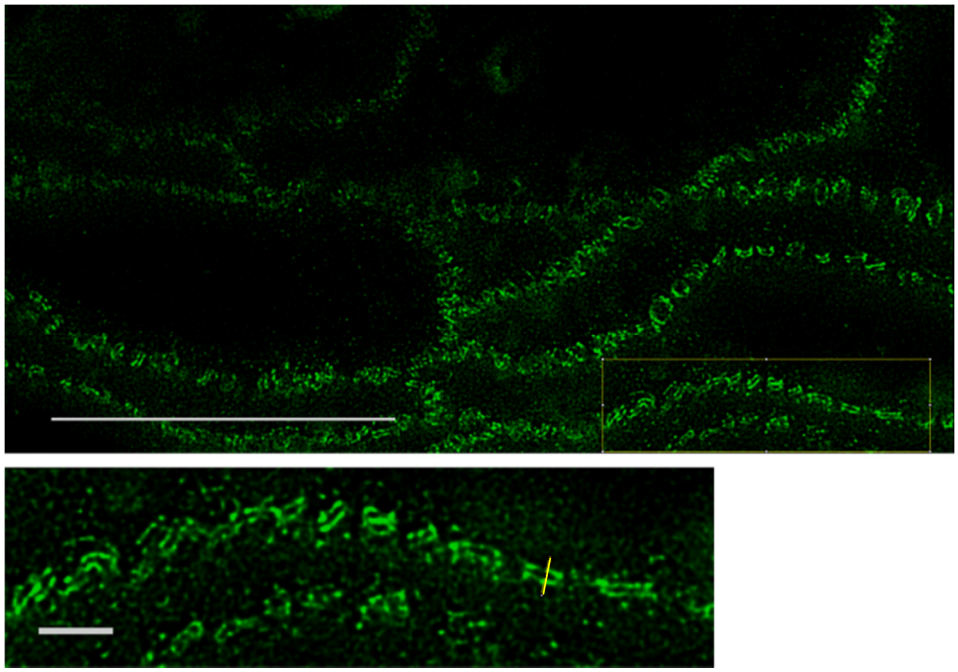

Figure 37: STED images of desmoplakin in SS labeled by immunolabeling. (Top – scalebar is 10 µm) The bottom image shows a zoom of the marked area in the top image. (Bottom – scalebar is 1 µm)

The fibrous protein keratin is now investigated. One of the keratin types present in the epidermis is keratin 1 and this is therefore labeled through immunolabeling. The resulting image is expected to show labeling of the corneocytes in the SC. It is also expected to label the keratin inside the cells in the underlying layers but the focus will be on the corneocytes. The thickness of these corneocytes is said to around 500 nm. Images of the sample is taken using the Leica system but only using confocal microscopy as the structure in question is expected to be larger than the resolution limit. The resulting image (Figure 38) shows that the outermost part of the SC has not been labeled while the inner part has been. This may due to the dyes inability to penetrate the dense corneocytes as these become denser closer to desquamatizing. The thickness of the corneocytes is measured in the same manner as the desmoplakins. Three of these are measured and the average thickness is found to be around 500 nm.

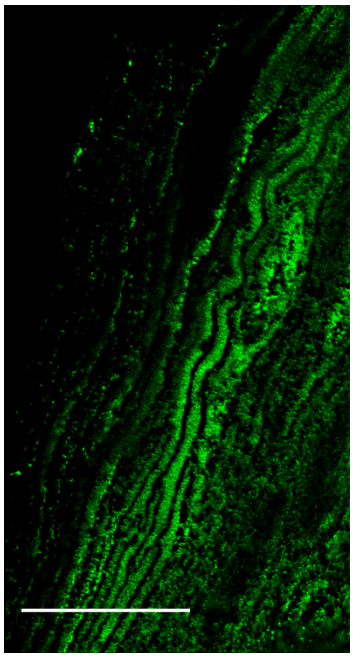

Figure 38: STED image of keratin 1 in the SC labeled by immunolabeling. The egde of the SC can be seen to the left. Scalebar is 10 µm.

4. Conclusion

The conclusions drawn from the results above will now be stated.

4.1 Characterization of the Leica STED system

The measured diameter of the PSF of the Leica system was found to be 200±10nm. This confirms to Abbé's law of diffraction (2.5), showing that the system operating at the diffraction limit. The PSF for the STED laser was donut shaped. The intensity is not evenly distributed as it appears weaker at the lower right side of the donut most likely due to a crooked sample placement. The minimum of the donut was not zero. It was measured to be 15% of the intensity of lowest intensity measured in the donut ring. The maximum of the PSF of the excitation laser matches the minimum of the PSF of the STED laser in both the x- and y-direction. The non-zero intensity of the STED donut, will cause some depletion at the center reducing the intensity and resolution of the system. These measurements show that it is important to characterize the optical properties of the system in order to understand the performance of the system.

When testing the resolution of the Leica system by using fluorescent beads with a diameter of 25 nm one achieves a resolution at approximately 30 nm. The resolution is maximized as the intensity of the STED laser increases which confirms (2.7). This is also the case for fluorescent beads with a diameter of 47 nm. Fluorescent beads with a diameter of 20 nm from Invitrogen are not suited for STED microscopy as the increase in resolution happens at a much slower rate. It is concluded that although the shape of the STED laser was suboptimal it was still possible to achieve a resolution down to 30nm FWHM, which is close to the theoretical limit of the system. [35].

4.2 Affinity labeling and effects of DMSO

DMSO as a transdermal transport enhancer was tested using the Leica system. For the hydrophobic dye TopFluor DPPE an increased labeling of the skin samples is observed with an increased concentration of DMSO. This enhancement is also concentration dependent as a significant effect is observed at DMSO concentrations above 50 %. The optimum labeling of the SC with TopFluor DPPE is achieved when the dye is dissolved in 100 % DMSO. DMSO does not increase the amount of labeling with the hydrophobic dye ATTO 488 DPPE which could indicate that the dye has a higher affinity for DMSO than the sample. The optimal labeling is achieved when ATTO 488 DPPE is dissolved in 100 % PBS buffer. It was also seen that while TopFlour DPPE stained the SC well, ATTO 488 DPPE partitioned mostly to the lipid membranes of the lower layers of the epidermis.

When the skin samples are cut in 30 µm thick samples the SC has a tendency to swell during labeling making it difficult to image the entire epidermis at once. If skin samples are cut 10 µm thickness the SC does not swell as much but structures within the epidermis become difficult to visualize. The optimum thickness of the skin samples is therefore 20 µm.

Knowing the most optimal labeling technique for the hydrophobic dyes STED microscopy was applied to the samples and compared to confocal microscopy. By labeling with the hydrophobic dyes ATTO 488 DPPE and TopFluor DPPE the width of the intercellular lipids in the SC were measured to be around 200 nm when imaging with confocal microscopy suggesting that they are not resolved as 200 nm is the resolution limit of the system. Using STED these the intercellular lipids are found to have a thickness of around 100 nm and new structures becomes visible due to the improved resolution. If the STED intensity were to be increased further the resolution would be further improved but the samples were destroyed at higher STED power.

To visualize the entire epidermis the samples were labeled with both hydrophilic and hydrophobic dyes. The hydrophilic being Rhodamin B, ATTO 647 N and Abberior Star 440 SX and the hydrophobic being TopFluor DPPE and ATTO 488 DPPE. In general SB live cells are visible and the cellular nucleus can be distinguished. It can be seen that the cells flatten throughout the epidermis as they differentiate. The cellular nucleus can be observed until the SG. The hydrophilic dye Rhodamin B has a tendency to label keratin which can be seen as train tracks in the underlying layers. In the SC this dye labels both the corneocytes and the lipid matrix as the labeling in this layer appears smeared. The same is observed in SC with the dye ATTO 647N, but there was no labeling of keratin in the underlying layers. With Abberior Star 440 SX a more structural labeling of SC is observed but labeling of keratin is observed in the underlying layers.

The pathways through the SC are still not fully understood, especially the intracellular path way is still not fully accepted or understood. [12] Using the hydrophobic and hydrophilic dyes combined with STED microscopy the transport pathways through the skin can be visualized. When applying TopFluor DPPE on intact skin before slicing the dye was found not to penetrate the SC. If the sample on the other hand is labeled with Rhodamin B on intact skin before slicing and the hydrophobic dyes on the sliced skin it can be seen that both dye types use the intercellular pathway. Hydrophobic dyes applied after slicing are seen to pass through the lipid matrix in the SC. Rhodamin B labeled after slicing labels the entire SC both the corneocytes and the lipid matrix. This suggest that Rhodamin B has access to the intracellular space and thus can possible use an intercellular pathway to penetrate the sample. This could

be due to the polar nature of the molecule and its small size but also the high level of hydration of the skin when labeled after sectioning could play an important role. Under normal circumstances little or no free water is available in the SC. [15] However during the labeling process of the sliced samples the skin is submerged in water for hours. This was seen to induce swelling of the SC and to free water being available in the corneocytes. Samples labeled with Abberior Star 440 SX after slicing as well as the hydrophobic dyes also shows use of the intercellular pathway. It is interesting to note the difference in behavior of the Abberior Star 440 SX and the Rhodamin B. While the Abberior star 440 SX is confined to the intercellular path way Rhodamin B can penetrate the corneocytes. This shows the complicated nature of the skin barrier and could well be due to the smaller size of the Rhodamin B.

In order to examine specific structures within the epidermis the proteins desmoplakin and keratin 1 were labeled by immunolabeling. The density of desmoplakin is quite low in the SC but considerably higher in the underlying layers. Desmoplakin occur in pairs on each side of the intercellular space. The average distance between two placks is 160 ± 30nm and a resolution down to 40 nm was achieved. This value is in reasonable agreement with results previously measured using TEM. [15] Keratin 1 was also imaged and can be seen in the corneocytes in the SC and these have an average thickness of around 500 nm.

In conclusion the work presented in this thesis show that super resolution optical microscopy is a valuable new tool to study the structure and penetration pathways of human skin. It was shown for the first time that STED microscopy could resolve the intercellular lipids as well as individual proteins in human skin. The results presented suggest show great promise for future work enabling investigating of interactions of penetrating molecules with individual proteins.

5. References

1. Kirschner, N., et al., *Contribution of Tight Junction Proteins to Ion, Macromolecule, and Water Barrier in Keratinocytes.* Journal of Investigative Dermatology, 2013. **133**(5): p. 1161-1169.
2. Madison, K.C., *Barrier function of the skin: "La Raison d'Etre" of the epidermis.* Journal of Investigative Dermatology, 2003. **121**(2): p. 231-241.
3. Erni, R., et al., *Atomic-Resolution Imaging with a Sub-50-pm Electron Probe.* Physical Review Letters, 2009. **102**(9).
4. Arroyo-Camejo, S., et al., *Stimulated Emission Depletion Microscopy Resolves Individual Nitrogen Vacancy Centers in Diamond Nanocrystals.* Acs Nano, 2013. **7**(12): p. 10912-10919.
5. *The Nobel Prize in Chemistry 2014* 2014 21-08-2015]; Available from: http://www.nobelprize.org/nobel_prizes/chemistry/laureates/2014/.
6. Ng, S.-F., et al., *Validation of a Static Franz Diffusion Cell System for In Vitro Permeation Studies.* Aaps Pharmscitech, 2010. **11**(3): p. 1432-1441.
7. Klang, V., et al., *In vitro vs. in vivo tape stripping: Validation of the porcine ear model and penetration assessment of novel sucrose stearate emulsions.* European Journal of Pharmaceutics and Biopharmaceutics, 2012. **80**(3): p. 604-614.
8. Hans Schaefer, T.E.R., *Skin Barrier - Principles of Percutaneous Absorption*. 1996: Karger.
9. William Montagna, A.M.K., Kay S. Carlisle, *Atlas of Normal Human Skin*. 1992: Springer-Verlag.
10. Lowell A. Goldsmith, M.D., *Biochemistry and Physiology of the Skin.* 1983. **1**: p. 3-197.
11. Garrod, D.R., *Desmosomes and hemidesmosomes.* Current Opinion in Cell Biology, 1993. **5**(1): p. 30-40.
12. Ishida-Yamamoto, A. and S. Igawa, *The biology and regulation of corneodesmosomes.* Cell and Tissue Research, 2015. **360**(3): p. 477-482.
13. Nemes, Z. and P.M. Steinert, *Bricks and mortar of the epidermal barrier.* Experimental and Molecular Medicine, 1999. **31**(1): p. 5-19.
14. Proksch, E., J.M. Brandner, and J.M. Jensen, *The skin: an indispensable barrier.* Experimental Dermatology, 2008. **17**(12): p. 1063-1072.
15. North, A.J., et al., *Molecular map of the desmosomal plaque.* Journal of Cell Science, 1999. **112**(23): p. 4325-4336.
16. Forslind, B., et al., *A novel approach to the understanding of human skin barrier function.* Journal of Dermatological Science, 1997. **14**(2): p. 115-125.
17. Scheuplein, R.J., *Permeability of the skin.* Comprehensive Physiology, 2011.
18. Couto, A., et al., *Dermic diffusion and stratum corneum: A state of the art review of mathematical models.* Journal of Controlled Release, 2014. **177**: p. 74-83.
19. Wang, T.F., G.B. Kasting, and J.M. Nitsche, *A multiphase microscopic diffusion model for stratum corneum permeability. I. Formulation, solution, and illustrative results for representative compounds.* Journal of Pharmaceutical Sciences, 2006. **95**(3): p. 620-648.
20. Lane, M.E., *Skin penetration enhancers.* International Journal of Pharmaceutics, 2013. **447**(1-2): p. 12-21.

21. Joachim W. Fluhr, P.E., Enzo Berardesca, Howard I. Maibach, *Bioengineering of the Skin: Water and the Stratum Corneum*. 2005: CRC Press.
22. Barry, B.W., *Mode of action of penetration enhancers in human skin.* Journal of Controlled Release, 1987. **6**(1): p. 85-97.
23. Williams, A.C. and B.W. Barry, *Penetration enhancers.* Advanced Drug Delivery Reviews, 2012. **64**: p. 128-137.
24. Cox, G., *Optical Imaging Techniques in Cell Biology*. 2007: Taylor & Francis.
25. Walla, P.J., *Modern Biophysical Chemistry - Detection and Analysis of Biomolecules*. 2 ed. 2014: Wiley-VCH.
26. Max Born, E.W., *Principles of optics - Electromagnetic theory of propagation, interference and diffraction of light*. 7th ed. 1999: Cambridge University Press.
27. Pawley, J.B., *Handbook of Biological Confocal Microscopy*. 3rd ed. 2006: Springer.
28. Alioscka A. Sousa, M.J.K., *Nano Imaging - Methods and Protocols.* 2013: p. Chapter 5.
29. U. Valentin Nägerl, A.T., *Nanoscale Imaging of Synapses*. 2014.
30. Ramos-Vara, J.A., *Technical aspects of immunohistochemistry.* Veterinary Pathology, 2005. **42**(4): p. 405-426.
31. Harke, B., et al., *Resolution scaling in STED microscopy.* Optics Express, 2008. **16**(6): p. 4154-4162.
32. Ward, R.K., et al., *Evaluation in vitro of epidermal cell keratinization.* Toxicology in Vitro, 1997. **11**(5): p. 633-636.
33. Sun, T.T. and H. Green, *IMMUNOFLUORESCENT STAINING OF KERATIN FIBERS IN CULTURED-CELLS.* Cell, 1978. **14**(3): p. 469-476.
34. Bos, J.D. and M. Meinardi, *The 500 Dalton rule for the skin penetration of chemical compounds and drugs.* Experimental Dermatology, 2000. **9**(3): p. 165-169.
35. Vicidomini, G., et al., *STED Nanoscopy with Time-Gated Detection: Theoretical and Experimental Aspects.* Plos One, 2013. **8**(1).

6. Appendix

6.1 Appendix 1: Protocols

1. Protocol for cryofreezing skin samples:

1) Add liquid nitrogen to a flamingo container so the bottom is covered
2) Pour isopentane in a metal beaker and place in the container with liquid nitrogen
3) Apply Tissue Tek in the bottom of a plastic petri dish
4) Place a skin sample in the petri dish and add Tissue Tek again
5) Now place the skin sample inside the metal beaker – wait 1 min.
6) Place the frozen skin sample in designated container and place this inside a container with dry ice.

2. Protocol for PVA bead samples (aka gold nanoparticles)

1) Dissolve about 4,5 g PVA (Mowiol 4-88) in 30 mL milliQ water, stir and heat to about 50°C to ease the dissolution
2) Pipet a small volume of the gold nanoparticles (300 µL) into an Eppendorf cup and sonicate for 15 min.
3) Dilute 60 µL of the sonicated gold nanoparticles into a new Eppendorf cup and dilute with 200 µL PVA (this volume is enough for about one slide)
4) Sonicate the solution for about 10-15 min.
5) Pipet 200 µL of the solution onto to coverslip (Ø 24 mm) and spincoat for 2000 rpm for about 40 seconds.
6) Dry (overnight) in vacuum chamber
7) Mount the coverslip on a microscope slide using PVA.

3. Protocol for cleaning cover slips in basic piranha:

Basic piranha solution 1:5:5: 150 mL milliQ water, 30 mL 30 % hydrogen peroxide, 30 mL ammonium hydroxide

1) Place coverslips in designated holder
2) Place holder in basic piranha for 1-1,5 hours at around 80°C
3) Rinse with milliQ water
4) Dry in 90°C oven (overnight)

4. Protocol for fluorescence polystyrene beads (Duke scientific/Thermo, 1% solid)

1) Pipet a small volume and dilute in milliQ water to a stock solution in an Eppendorf cup, 1:500. Sonicate for 10-15 min.
2) Add 300 µL Polylysine solution to each coverslip. After 10 min, rinse in milliQ water and dry using N_2.
3) Dilute the PS sphere solution to the final concentration in milliQ water. The concentration depends on the size:
    a. Ø 20 nm: 1:5000, 1:50.000, 1:1.000.000
    b. Ø 25 nm: 1:5000, 1:50.000, 1:1.000.000
    c. Ø 47 nm: 1:5000, 1:100.000
4) Add about 300 µL of the PS bead solution to each coverslip, wait for 10 min, rinse and dry as above.
5) Mount the coverslip on a microscope slide using 5-7 µL ProLong Gold.

5. Protocol for preparing coverslips for skin samples:

1) Add 300 µL poly-L-lysine – wait 15-20 min.
2) Rinse with milliQ water
3) Dry in 90°C oven (2 hours)

6.2 Appendix 2: Dyes

Amphiphilic dyes:

Table 1: Data sheet for the amphiphilic fluorescent molecule TopFluor DPPE.

Dye	TopFluor DPPE
Molecular structure	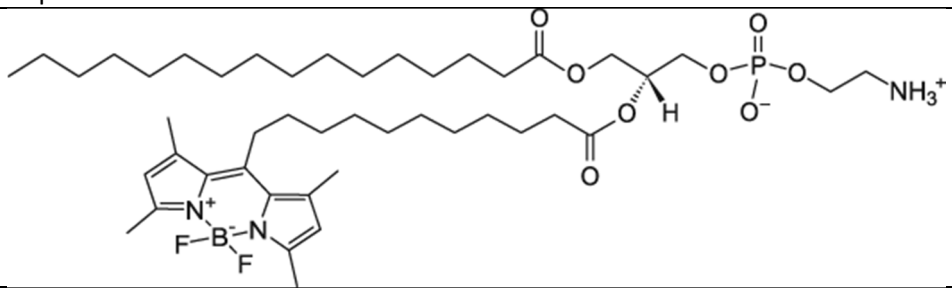
MW [g/mol]	867,890
$\lambda_{ex}/\lambda_{em}$ [nm]	495 / 503
Absorption & Fluorescence Spectrum	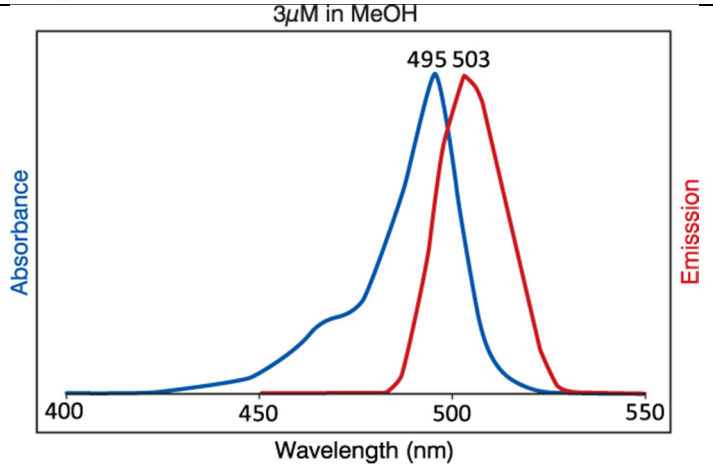 Data taken from the company website: http://www.avantilipids.com/index.php?option=com_content&view=article&id=1963&Itemid=635&catnumber=810282

Table 2: Data sheet for the amphiphilic fluorescent molecule ATTO 488 DPPE.

Dye	ATTO 488 DPPE
Molecular structure	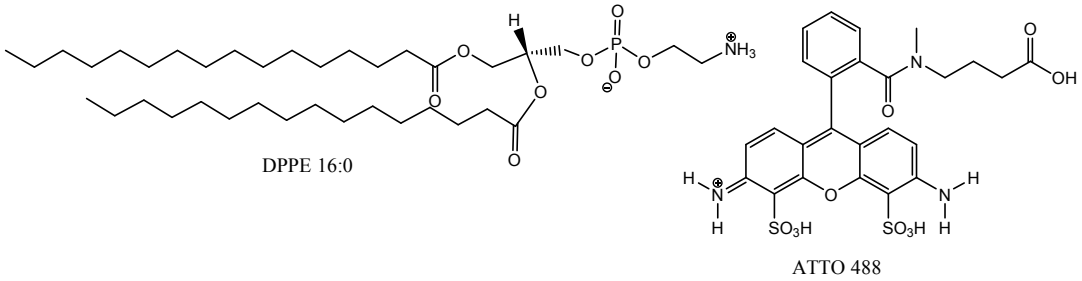
MW [g/mol]	1263
$\lambda_{ex}/\lambda_{em}$ [nm]	501 / 523
Absorption & Fluorescence Spectrum	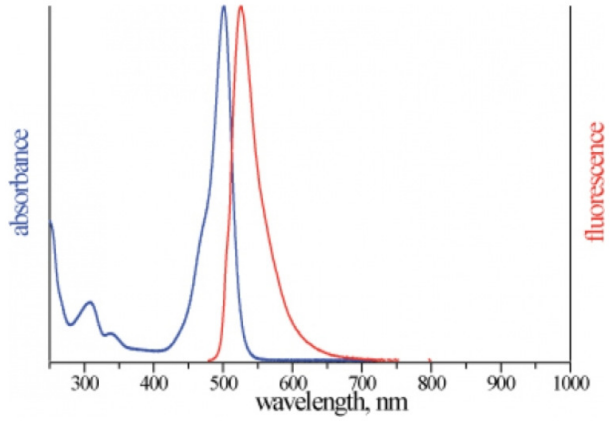 Data taken from the company website: https://www.atto-tec.com/attotecshop/product_info.php?info=p99_atto-488.html

Hydrophilic dyes:

Table 3: Data sheet for the hydrophilic fluorescent molecule Rhodamin B:

Table 4: Data sheet for the hydrophilic fluorescent molecule ATTO 647N:

Dye	Rhodamin B	ATTO 647 N
Molecular structure	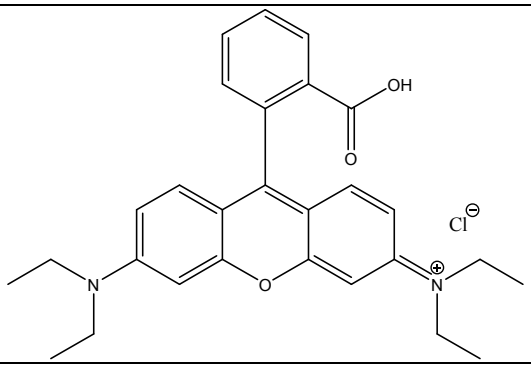	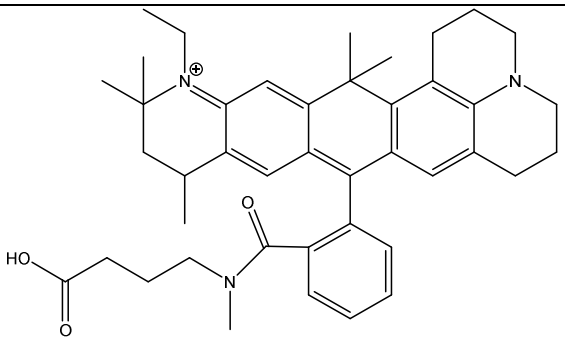
MW [g/mol]	479,01	746
$\lambda_{ex}/\lambda_{em}$ [nm]	554 / 580	644 / 669
Absorption & Fluorescence Spectrum	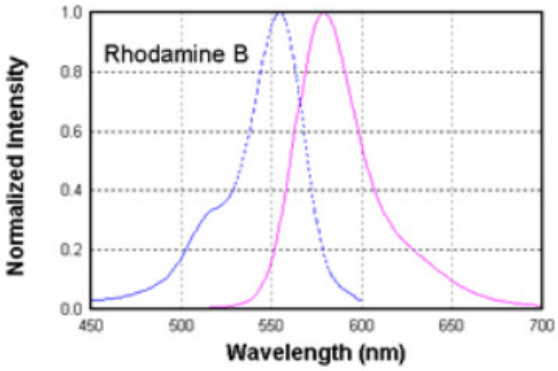 *Absorption (blue), fluorescence (pink)* Data taken from the company website: *http://www.sigmaaldrich.com/catalog/product/sigma/r6626?lang=en&region=DK* Spectrum taken from the following website: http://www.iss.com/resources/research/technical_notes/PC1_PolarizationStandards.html#.	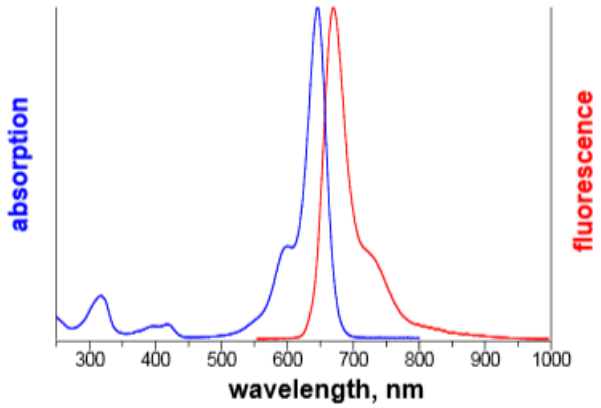 Data taken from the company website: http://www.atto-tec.com/attotecshop/product_info.php?language=en&info=p114_atto-647n.html&

Table 5: Data sheet for the hydrophilic fluorescent molecule Abberior Star 440 SX.

Dye	Abberior Star 440 SX
Molecular structure	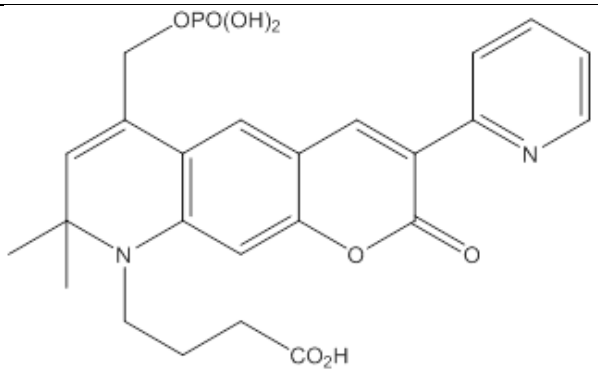
MW [g/mol]	597,2
$\lambda_{ex}/\lambda_{em}$ [nm]	436 / 515
Absorption & Fluorescence Spectrum	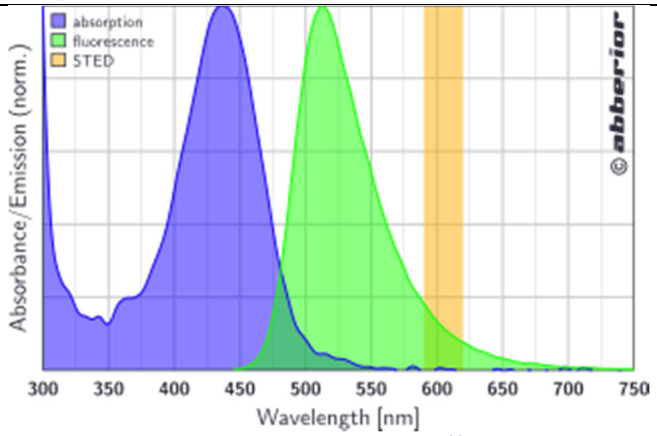 Data taken from the company website: http://www.abberior.com/products/productlist/prod/abberior-star-440sx/

6.3 Appendix 3: Figures

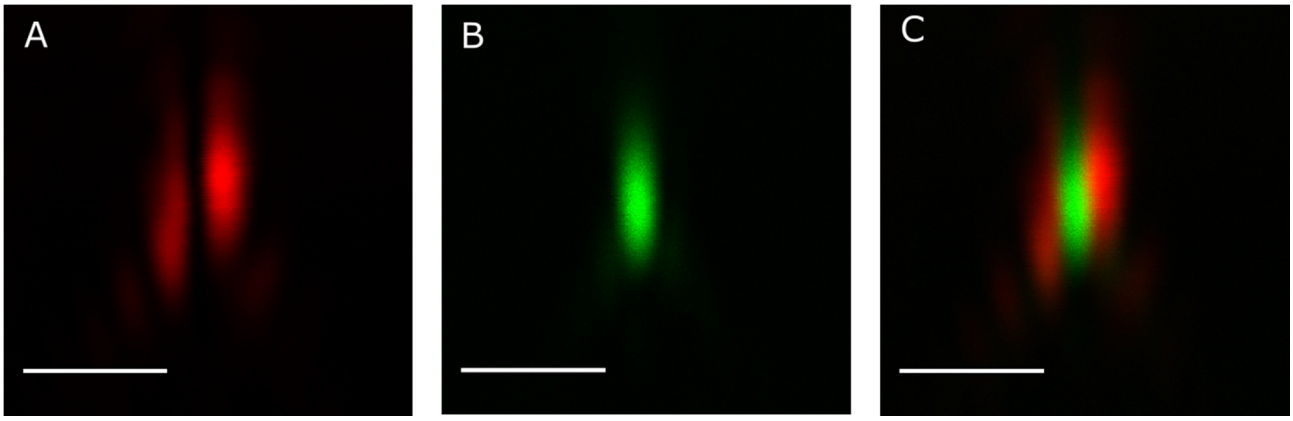

Figure A3.1: The PSFs in xz-direction of the STED laser and excitation laser of the Leica system viewed using gold nanoparticles. A) PSF of the STED laser. B) PSF of the excitation laser C) The two PSFs combined. Scalebar is 1 µm.

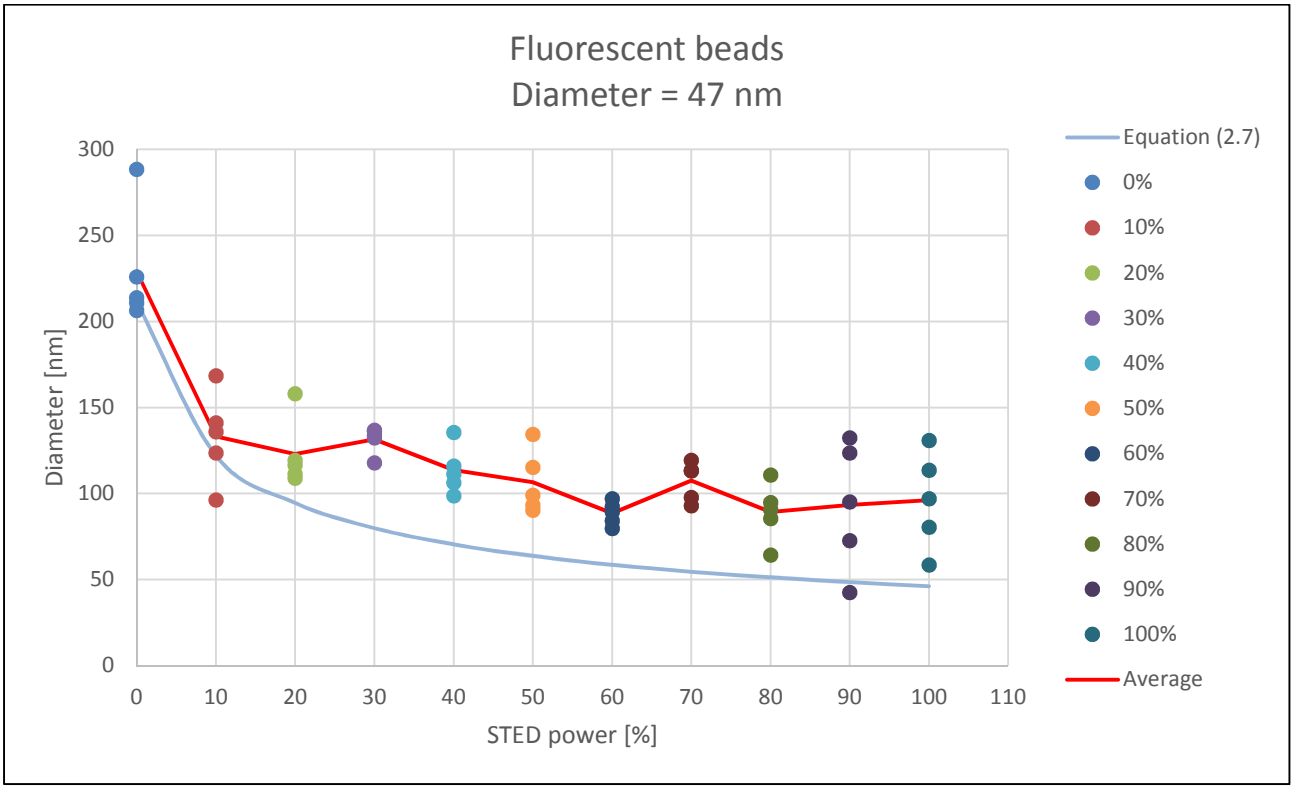

Figure A3.2: The diameter [nm] of 47 nm fluorescent beads as a function of the STED intensity [%]. For each STED intensity 5 bead diameter measurements are made and plotted. The average of the diameters is also plotted. Equation (2.7) is plotted with the following values: $\frac{I_{STED}}{I_S} = 40$ for I_{STED}=100%, λ=592 nm and NA=1,4.

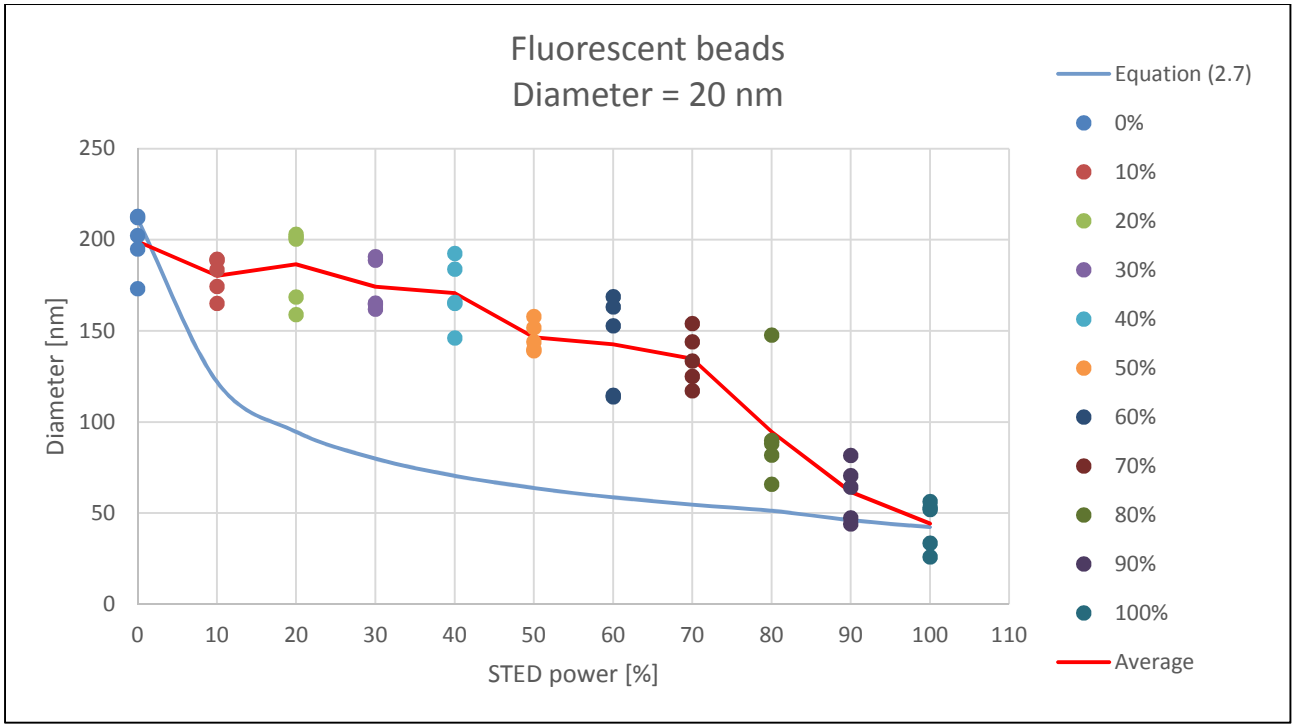

Figure A3.3: The diameter [nm] of 20 nm fluorescent beads as a function of the STED intensity [%]. For each STED intensity 5 bead diameter measurements are made and plotted. The average of the diameters is also plotted. Equation (2.7) is plotted with the following values: $\frac{I_{STED}}{I_S} = 40$ for I_{STED}=100%, λ=592 nm and NA=1,4.

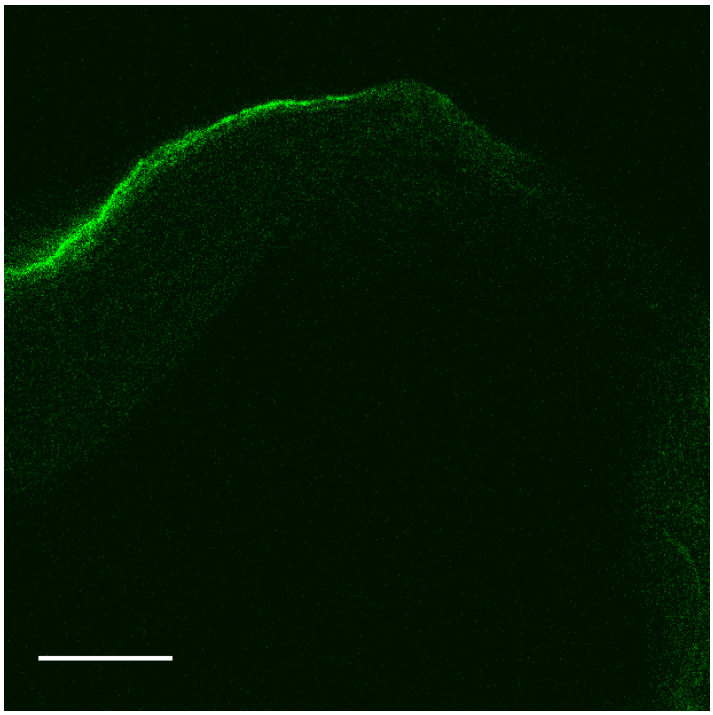

Figur A3.4: Confocal image of the epidermis labeled with TopFluor DPPE on intact skin before slicing. SC can be seen at the top. Scalebar is 10 µm.

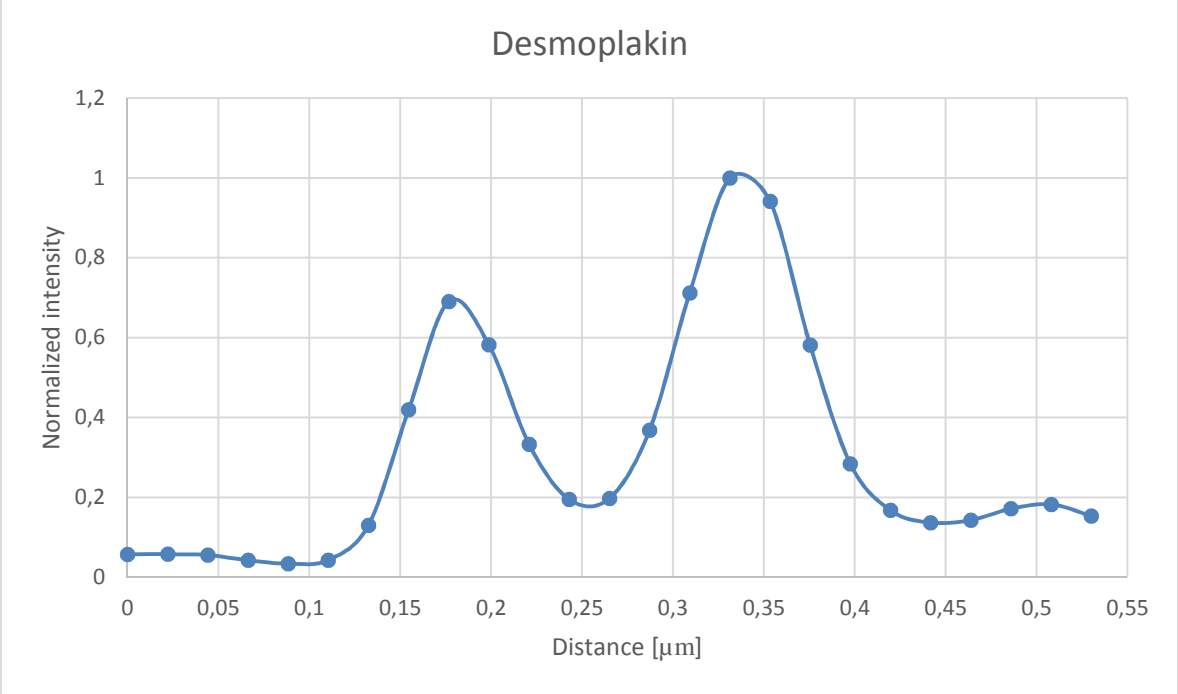

Figur A3.5: Plot profile showing the normalized intensity as a function of the distance [µm] created along the drawn line in the bottom image in Figure 37.